2011

A Concept for Direct Control of Rotary Blood Pump Speed by Inlet Pressure

Ibrahim Seven
Cleveland State University

A CONCEPT FOR DIRECT CONTROL OF ROTARY BLOOD PUMP SPEED BY INLET PRESSURE

IBRAHIM SEVEN

Bachelors of Science in Mechatronics Engineering,

Bahcesehir University, Istanbul, Turkey

August, 2010

Submitted in partial fulfillment of requirements for the degree

MASTER OF SCIENCE IN BIOMEDICAL ENGINEERING

at the

CLEVELAND STATE UNIVERSITY

May, 2011

This thesis has been approved
For the Department of Chemical and Biomedical Engineering
and the College of Graduate Studies by

_____

Thesis Chairperson, Dr. William A Smith

_____

Department & Date

_____

Dr. Murad Hizlan

_____

Department & Date

_____

Dr. Dan J. Simon

_____

Department & Date

To my family members: Salih Seven, Katibe Seven, Ecem Seven, and Merve Begum Erdir.

ACKNOWLEDGEMENTS

I would like to thank my advisor and mentor Dr. William A. Smith for his full support and guidance in this project. He has been very kind and patient while suggesting to me the outlines of this project and correcting my mistakes. He always motivated me and believed in my skills. I would also like to thank my committee members, Dr. Murad Hizlan and Dr. Dan J. Simon for their insight and knowledgeable support during my research.

I would like to acknowledge my professor Dr. Ana Stankovic for her tremendous help during this project. I would like to thank Chemical and Biomedical Engineering Department faculty members Dr. Orhan Talu, Dr. Nolan Holland and Dr. Joanne Belovich for their guidance during my entire Master's study. I would also acknowledge our department staff Ms. Becky Laird and Ms. Darlene Montgomery for their effort to make me feel home.

Finally, I would like to thank Cleveland Clinic Principal Engineer Mr. Dave Dudzinski, Cleveland State University Physics department technician Mr. Bryan Carpenter and my friend Mr. Alper Aksu for their significant help during this thesis study.

A CONCEPT FOR DIRECT CONTROL OF ROTARY BLOOD PUMP SPEED BY INLET PRESSURE

IBRAHIM SEVEN

ABSTRACT

Heart failure remains a major health problem for the world. Heart transplantation is the most effective treatment for end stage heart failure. A major problem with heart transplantation is finding adequate numbers of appropriate donors. The lack of donor numbers in the world creates a significant clinical need for blood pumping devices. The ability of ventricular assist devices to relieve the consequences of less than terminal heart failure further creates a need for assist therapy. Current new ventricular assist devices are built around continuous flow technology. These nonpulsatile assist devices have had major clinical success in relieving symptoms and increasing patient survival. However they have a control issue as opposed the first generation pulsatile Ventricular Assist Devices (VADs) in that their output is sensitive to pressure difference, not primarily to inlet pressure. We have developed a rotodynamic blood pump speed management concept that results in a pump that responds to inlet pressure in a Starling law-like manner without active electronic controls or pressure sensors. The long term goal of this project is to develop a VAD system which responds as the natural human heart does. The pump speed is controlled by an adjunct electromechanical inlet conduit.

The inlet conduit has 2 integrated cylinders. The inner cylinder is the blood flow pathway, and is flexible in order to expand/collapse in response to inlet blood pressure. The outer cylinder is used as the coil of a tank circuit. There is also a ferrofluid reservoir which is connected to the space between the 2 cylinders. The majority of ferrofluid is in the reservoir when inlet pressure is high, but ferrofluid flows into the core of the coil when inlet pressure is low. The inductance of the coil varies in response to the volume of the ferrofluid within the core. Therefore the natural frequency of the tank circuit varies and the impedance of the tank circuit changes. The control circuit is connected in series with the motor leads. Thus the voltage change across the control circuit directly controls the amplitude of the voltage across the motor leads. The motor speed changes in response to the amplitude of the voltage change. The system is operated at 10 MHz frequency in order to minimize the component size and maximize the Q factor.

The specific aims of this thesis are to:

1) Explore the elementary feasibility of this tank circuit concept
2) Explore and define the issues that will be involved for developing such systems in the future.

TABLE OF CONTENTS

LIST OF TABLES

LIST OF FIGURES

CHAPTER 1

BACKGROUND AND SIGNIFICANCE

1.1 Need for Ventricular Assist Device

Heart disease remains the single largest health problem in the United States. Coronary artery disease is the most common cause of death for both males and females, claiming over 450,000 lives annually and is a contributor to hundreds and thousands of additional deaths [1]. Heart failure is a common cause of death in many clinically relevant scenarios, e.g., as a complication of myocardial infarction, due to primary myocardial diseases (cardiomyopathies, myocarditis) or as a complication of cardiac surgical or catheter interventional procedures. Numerous studies have shown the need for cardiac assist and replacement devices; in fact, one Institute of Medicine study estimates 35,000

to 75,000 patients within the United States could have a prolonged life with some form of cardiac device [2]. An NIH workshop placed the potential patient need at roughly 100,000 cases per year [3]. The same report notes that there is no reason to believe that the original disease state has to be arrested by VAS (Ventricular Assist System) implant, an important point for system designs that depend on myocardial function as part of the operational logic. All studies emphasize the importance of quality of life; meaning a truly valuable VAS implant should not just result in survival but permit rehabilitation of the patient to an active and satisfying life.

1.2 Advantages of Rotary Dynamic Blood Pumps, and Control Issue of these Pumps

1.2.1 Rotary Dynamic Pump Advantages-Disadvantages

The clinical need for blood pumping has a wide range of applications, from permanent, total artificial hearts (TAHs) to short-term, partial circulatory support required for minimally invasive cardiac surgery or interventional cardiology procedures. Ventricular assist systems have been built around rotary dynamic (rotodynamic) pumps of axial, mixed flow or radial flow geometry. These have shown significant success with respect to saving lives and improving the quality of life of heart disease patients. One limitation, however, of this approach to building a blood pump is that rotodynamic

pumps are sensitive to pressure difference and not independently to inlet and outlet pressures. In this respect they differ from successful pulsatile VADs and the natural heart, where inlet pressure effects on flow output are much greater than outlet pressure impacts.

A number of continuous flow pumps have been used successfully including the DeBakey VAD (MicroMed Technologies Inc., Houston, TX), the Jarvik 2000 Flowmaker (Jarvik Medical, Inc., New York, NY), and the HeartMate II (Thoratec Corp., Pleasanton, CA) [4-5]. These devices share many design similarities: an axial flow impeller is mounted on a rotor, which is supported fore and aft on pivot points. The most recently clinically approved design, the HeartMate II, is the biggest and slowest turning of these axial flow, pivot point supported pumps. This pump received a PMA (Premarket Approval) permitting commercial sale for bridge to transplant [5]. It is now in broad clinical use.

The VentrAssist LVAD (Ventracor Ltd., Chatswood, AUS), and the CorAide (formerly, Arrow International, Reading, PA)) are examples of radial flow pumps with blood lubricated, hydrodynamic bearings that have seen clinical trials [6, 7].

Circulite has a miniature pump design in clinical trial [8]. The impeller is supported on a conical blood lubricated bearing and magnetically coupled to the motor, which is intended to be a “pacemaker pocket” implant. Another device, the CorAide, saw clinical

trials in Europe. The CorAide is a Cleveland Clinic (CCF) technology, co-invented by this thesis's supervisor, which has provided extensive experience to guide future blood pump development efforts [9-10]. The Arrow effort was terminated by that corporation's financial difficulties, but another company has picked up the technology, and more recently Ventracor has been financially distressed. Overall it appears that financial burdens have hindered the progress of both of these devices.

The Hemopump was an earlier attempt to develop an intravascular device that could provide greater circulatory support than the IABP [11]. The Hemopump was a catheter-mounted, axial-flow pump that had the pump inlet in the left ventricle and the outlet located in the aorta. A spinning, "bicycle-brake" cable rotated the impeller inside the catheter while purge fluid was required to lubricate the cable-catheter interface and pump seal. The Impella Recover LP [Abiomed, Danvers, and Mass] is another catheter-based pump that incorporates a miniature motor at the pump end, eliminating the spinning cable [12, 13].

Purge fluid is still required, creating a potential failure mode as well as providing a pathway for circulatory bacterial infection. FDA approval for commercial sale has recently been granted via a 510K [14]. Current FDA approval is only for six hours of use.

A fundamentally different approach to blood pump bearing design employs magnetic support for the rotating elements. The DuraHeart (Terumo, Michigan) and the Incor

(Berlin Heart AG, Berlin, DEU) are VADs that have had clinical trials [15, 16]. WorldHeart (Toronto, ONT) has also performed least two primary clinical trials with an implantable pump, Levacor, designed by the Levitronics team (Waltham, MA). Levitronics has received a PMA for a temporary use, externally positioned magnetically levitated VAD, with preliminary reports of adequate pump performance [17].

Rotodynamic technology based pumps have been widely and aggressively pursued as a means of developing an implantable, successful VAD. However, all of these pumps have a penalty, relative to pulsatile pumps, with respect to the issue of adjustment to changes in physiologic demand.

1.2.2 Frank-Starling Response of the Natural Heart, and Good Pulsatile Assist Devices

Frank-Starling Law

The Frank-Starling law states that the cardiac output is dependent on venous return. In other words the volume of the blood which returns to heart determines the cardiac output by stretching the heart muscle fibers. This stretch and corresponding contractile force increases as cardiac output increases. According to the law, if the venous return decreases, contractile force will decrease, which will overall create a lower cardiac output [18]. **Figure 1** illustrates the ventricular output based upon venous return.

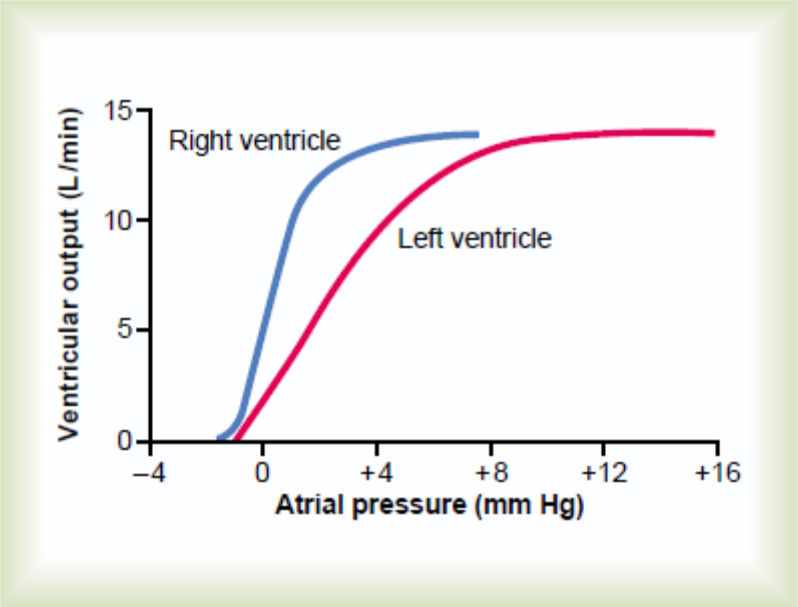

Figure 1 -- illustrates the cardiac output based upon the venous return. Taken from Guyton-Hall Medical Physiology text book [18].

Pulsatile Pumps

Pulsatile devices, such as the Thoratec and HeartMate VADs (Thoratec Corp., Pleasanton, CA), the BVS 5000 (ABIOMED, Danvers, MA), the Novacor LVAS (WorldHeart Inc., Oakland, CA) and the Berlin Heart VAD (Berlin Heart AG, Berlin, DEU), have proven track records in restoring patient cardiac output when used as a bridge to transplantation [19-20].

A characteristic of all of these pumps is that the filling phase is physically decoupled from the emptying phase. While the controller is in fill mode, the pump diaphragm floats with relatively little resistance to blood pressure. Venous return can fill the chamber with as much or as little blood as the body supplies, subject to the limits of the maximum chamber size and the time spent in fill phase. When the pulsatile VAD shifts to eject mode, the inlet valve closes, the outlet valve opens, and the power level is generally adequate to completely empty the chamber in the time allowed, before switching back to the filling phase. Most pulsatile VADs have a means to sense that the chamber is completely full so that the switch to eject can occur early, if venous return is high.

1.2.3 Pressure Flow Characteristics of a Rotary Dynamic Pump

Rotary dynamic pumps spin continuously and are pressure difference sensitive. Filling and emptying occur simultaneously, and there is no decoupling of the venous and aortic pressure effects. Rotation speed, flow, and pressure difference describe each operating point, as shown on the figure presenting a PediPump operating map. A physiologically very significant 5 mmHg increase in venous pressure would have the same effect on flow as a physiologically not so significant 5 mmHg drop in aortic pressure. The venous pressure increase might call for a doubling or more of flow; if the systemic pressure drop resulted from patient relaxation, no increase in flow, or a drop in flow, might be appropriate.

Figure 2 results from a recent Pedi Pump prototype mapping experiment and illustrates the pressure rise as a function of flow in liters per minute.

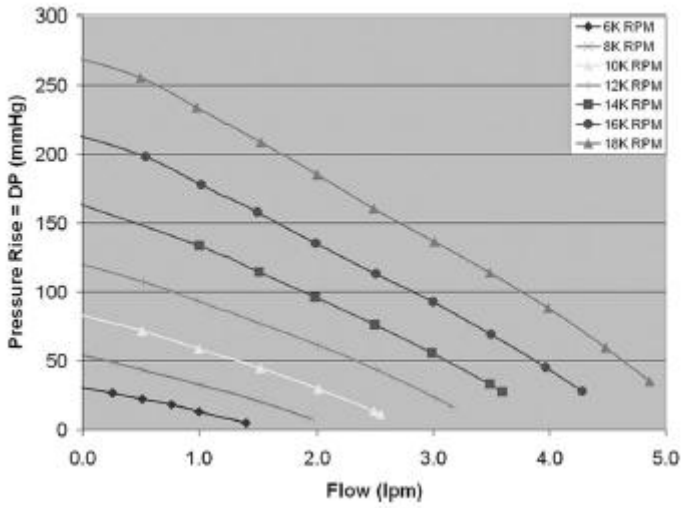

Figure 2 -- illustrates the pressure-flow characteristics of a rotary dynamic pump.

1.3 Prior Examples of Control Strategies

To address the fundamental limitation of rotodynamic pumps, various speed control strategies have been suggested, and in some cases implemented. The simplest pump control strategy is an open loop approach. Speed is adjusted manually, presumably by an "expert" who can look at the patient parameters, and make a suitable judgment. This has worked quite well for cardiopulmonary bypass, ECMO, and post-cardiotomy assist, where the patients are passive, usually unconscious.

This approach has also been used for implanted assist pumps, such as the Jarvik 2000, that are operated in partial assist mode [21]. The pump speed is set well below a critical point for suction, but high enough that regurgitation should not often be severe. The residual ventricular function takes care of variations in venous return. In stable patients with significant residual function, for whom only partial assist is necessary to achieve rehabilitation, this seems to restore net normal cardiac function. However, there still is a need for a device for patients who require permanent cardiac assist devices because they have limited recoverable myocardial function, and/or issues with rhythm. There are risks of events like dehydration, exsanguination, or valsalva-like transient abnormal restrictions of venous return, where these patients' health and safety will be compromised if the pump does not effectively respond to large changes in inlet conditions. End stage and "healthier" patients both will receive benefits from a more advanced device that provides a fuller rehabilitation, a device that will safely respond to a wider range of activity and conditions without fatigue or dyspnea. Overall, it is evident that a more potent control will be needed to reach the full potential of cardiac assist for the hundreds of thousands of patients experiencing cardiac disease.

The need for better control is implicitly recognized by many groups working in the area, many of which are associated with clinical VAS teams [22-23]. Efforts have been made to use pressure transducers, but have not been used clinically [24, 25].

Chronically implantable transducers that will measure the small changes in atrial pressure that are physiologically significant with long term reliability are still an area of ongoing research. An approach like this will always require additional wiring, hardware and software to implement. Flow transducers have been incorporated into implantable pumps, notably the Micromed device [26]. This adds cost, complexity and long term reliability issues to the system. Heuristic algorithms are used to evaluate the flow waveform, to determine if the measured flow is actually the correct flow.

Other control algorithms analyze the pump current trace to determine the pump operating state [27-28]. One might require that a certain minimum residual current pulsatility exist, suggesting that the ventricle is still ejecting enough to affect the pump pressure difference, which affects the flow, which has a strong relationship to current. The ventricle must have a reasonable contraction for this logic to succeed. More sophisticated analysis of the frequency composition of the current waveform can be used, to identify characteristic instabilities in the power draw associated with flows too close to reversing or too close to zero. These show good results in demonstration tests, but depend on long term relationships between power and flow that do not change due to wear or deposition in pump components or drift of electronics. High sensitivity and specificity have been reported, but it may be too late if the control method can only report after the pump has collapsed the ventricle.

All of these control methods, while relatively easy to implement, are inferring the proper running speed from non-physiologic parameters, and run the risk of inferential errors.

It is clear that most designs are not addressing another key issue, that being that the transient flow effects must be severe enough to affect pump electrical operation; because pump power efficiency is almost always less than 50%, only a small component of the total current is due to flow instabilities. In certain cases, a very sophisticated analysis of the current waveform can be implemented [29]. However, this is another form of current sensitivity. If the pump power supply, motor electronics and motor torque coefficient are very robust, they will result in nearly instantaneous changes in power in response to load changes, with little speed variation. In addition to this, a high mechanical inertia could similarly damp transient speed effects. One solution is described as a fusion of control methods, meaning it attempts to integrate multiple cardiac effects to obtain a stronger indication of physiologic condition. Overall, the interpretation of the various signals is more and more frequently depending on “expert” systems to finally select the speed setting, which relies heavily on the appropriateness of the selected decision making rules with constant fine tuning based on the priorities and judgments of the design “expert” and not native physiological cardiac function [30].

CHAPTER II

PROPOSED DESIGN APPROACH

2.1 Background of Design Approach

2.1.1 Brushless DC Motor

Virtually all implanted rotodynamic blood pumps utilize brushless, sensorless DC motors. In order to have a better understanding of the brushless DC motor technology this following section gives a basic definition of a brushless DC motor (BLDC), its commutation and excitation.

A brushless DC motor is a synchronous motor. A permanent magnet is mounted in the rotor. Armature windings are mounted in the stator. These physical characteristics of the BLDC motor have many advantages and make it highly preferable within some specific applications [31].

Advantages-Disadvantages

Since the armature windings are stationary, they are easier to cool. Due to the absence of mechanical commutator switches or brushes, the life cycle is longer than conventional brushed motors. The BLDC motor is able to reach higher speed and torque [32].

On the other hand, the absence of brushes or commutation switches causes an issue with start-up commutation logic and generating starting torque. Due to this disadvantage, the BLDC motor is mostly preferred for low starting torque applications [33].

Commutation

With the absence of mechanical commutator brushes, solid state switching is used in order to commutate the BLDC motor. Each phase winding is controlled by transistors. The transistors are turned on/off in order to excite the windings. The state switching is done based upon the rotor position [33].

BLDC Motor Drive

In order to drive the solid switching transistors, two different types of control techniques are used [33]. These control methods are:

1) Sensor Drive

2) Sensorless Drive

Sensor Drive

A position sensor is used in order to determine the rotor position to control which lead's transistor is turned on. Based on the position feedback two of the three phases are turned on, and the remaining phase is turned off. This drive method was the only method which was used before the discovery of the sensorless method. While the sensor drive system is simple and robust, in many applications it can be difficult to fit in the necessary components and wiring. At a cost of more complex electronics, the sensorless approach addresses these issues.

Sensorless Drive

The key concept in sensorless drive is detecting and processing the back EMF voltage [34]. The current applied through the powered armature windings, induces a counter voltage across the unpowered windings, which is called back EMF voltage. Since there is one idle lead and two active leads at any instant the back emf voltage is measurable through the idle lead instantaneously.

Based on the excitation, the back emf voltage can be trapezoidal or sinusoidal. Through the shape of their back emf voltage, brushless DC motors are categorized in two groups such as: Trapezoidal BLDC and Sinusoidal BLDC [34]. Crossing points of the back-EMF voltage can be used to determine rotor position and the timing of switching.

Excitation

Pure DC voltage can be used to drive a BLDC motor, but other approaches have advantages. Chopping the DC voltage into a square wave permits easy digital control of the motor speed. Pulse width modulation (PWM) is used to regulate the on-time of the square wave, controlling the power delivered to the motor. Assuming the base frequency is high enough, the motor essentially rectifies the variable pulse width DC into continuous DC of suitable levels.

The square wave drive system utilizes efficient digital control electronics to drive the BLDC. However the square wave form has its disadvantages such as high ripple torque.

A sine wave motor drive signal is a more efficient drive method than the square wave. When the brushless dc motor is excited by sine wave current, the BLDC motor shows better performance than conventional brushed DC motors. Also, the ripple torque is reduced by the sine wave excitation. However, in ordinary circumstances modulating the sine wave to produce variable speed is not as straightforward as varying the pulse width of the square wave, and this form of excitation is much less frequently used. In our unique application, this is not an issue.

2.1.2 Electrical Characteristics of a "Tank Circuit" Near Resonance

The electronic component of our design contains a parallel LC circuit, or tank circuit. The tank circuit is able to store electrical energy oscillating at its resonant frequency. The capacitor holds energy in the electrical field based upon the applied voltage, and the inductor holds energy in the magnetic field based upon the current through it [35]. If a charged capacitor is connected parallel to the inductor, the capacitor discharges through the inductor and builds a magnetic field on the inductor until its voltage reaches zero. However, if the voltage of the capacitor is zero, the current reversely flows from inductor through the capacitor, sourced by the magnetic field of the inductor, after the capacitor's voltage consumption. The impedance of the tank circuit varies with the closeness of the operating frequency to the resonant frequency. When they are very far apart, the impedance is near zero. When they are close, the impedance is extremely high, theoretically infinite.

Due to the features of the components of a theoretical LC circuit, there is no energy consumption; all energy is stored within the capacitor and inductor and merely transferred [36]. However the circulating currents flowing between capacitor and inductor can be very high and real tank circuits will see power losses in the component resistances.

LC circuits are commonly used within many applications such as tuners, filters, oscillators, and pulse generators.

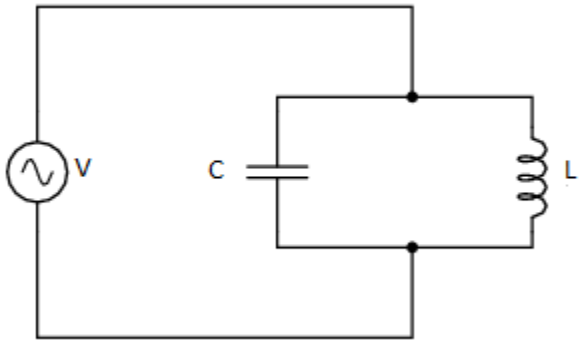

Figure 3 -- illustrates the schematic of no load tank circuit.

Resonance

The resonance point is where inductive reactance and capacitive reactance are equal. In order to observe the resonant behavior within the tank circuit, it must be driven by an AC signal. Resonant frequency of the tank circuit is calculated by equations 1 and 2 below:

$$\omega = \sqrt{\frac{1}{LC}} \tag{1}$$

$$f = \frac{1}{2\pi\sqrt{LC}} \tag{2}$$

where **L** is the inductance in henries, and **C** is the capacitance in farads. The angular frequency ω has units of radians per second.

The impedance of the tank circuit increases as the operating frequency of the system gets closer to the natural frequency, and it decreases as the operating frequency of the system gets further away from the natural frequency.

If the operating frequency of the system is equal to the natural frequency of the tank circuit, the impedance of the tank circuit becomes 'as high as possible,' also called infinite.

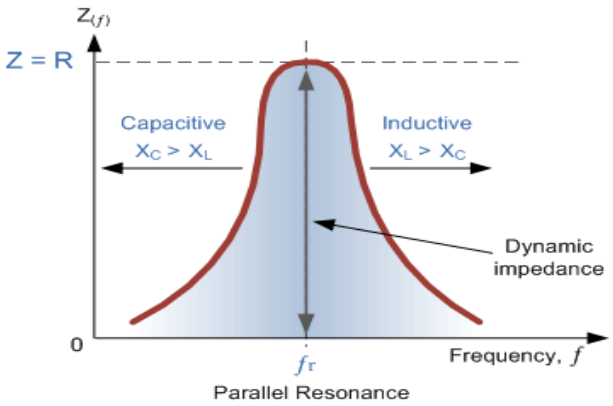

Figure 4 -- The electrical behavior of the tank circuit. The impedance curve peaks at the natural frequency.

2.1.3 Characteristics of Ferrofluid and Effects on Tuning of a Tank Circuit

Ferrofluid is a key component in this thesis. Ferrofluid, also known as magnetic fluid, is a colloidal suspension of single-type magnetic nanoparticles into the polar or nonpolar host carrier. The magnetic particles are approximately 10 nm in diameter. Since 1960, when this solution was synthesized, scientific studies and applications have been increasingly pursued [36].

The magnetic particles are coated by a surfactant to assist dispersion in solution. In terms of coating ferrofluid are categorized into two groups such as (SFF) Surfacted and (IFF) Ionic Ferrofluid [37].

The magnetization of the ferrofluid is mostly expressed by Brownian motions. Magnetic moments of the particles are calculated by the Maxwell equations [38]. We do not get into detail of those calculations and formulas in this thesis.

The viscosity of the ferrofluid is dependent to the percentage of the magnetic particles within the solution. The viscosity of the ferrofluid and the magneto viscous effect of the ferrofluid are proportional. The applications in which low viscosity is needed, the magneto viscous effect needs to be decreased. In our design the magnetoviscous effect is preferred rather than low viscosity.

Due to the high costs of EMG series ferrofluid from the Ferrotec Company, we ran our feasibility experiments with EFH1 series ferrofluid of Ferrotec Company which was already available at the Cleveland Clinic. EFH1 series of the ferrofluid has low viscosity and low magnetic saturation [39].

Figure 5 -- illustrates that the movement of the ferrofluid magnetic particle when an external magnetic field is applied

Applications

Ferrofluid is used within many applications such as: dynamic sealing, heat dissipation, inertial and viscous damper, and biomedical applications. We focused on biomedical applications rather than others.

Biomedical Applications

Ferrofluid is widely used within biomedical applications such as magnetic drug targeting, hyperthermia, contrast enhancement for magnetic resonance imaging, and magnetic separation of cells [36].

Because this would be ultimately an in vivo application, we focused on magnetic drug targeting rather than the others. This technique demonstrates the use of the ferrofluid inside of the human body.

Magnetic drug targeting: Since the ferrofluid could be oriented by the magnetic field vector lines, it is used for cancer tumor therapy. The idea is to concentrate the drug locally to tumor instead of dispersing drug to whole body. Within this application the ferrofluid is bound to drug. Focused magnetic fields concentrate the drug at the tumor. The ferrofluid will disperse within the whole body, after magnetic the field disappears. This ferrofluid spread is not harmful, due to the low amount of the ferrofluid is used and the basic biocompatibility of the colloidal iron and the carrier fluid.

Many experiments which focus on cancer healing have been conducted in rabbits and rats by this approach. Papers by Lübbe et al. [40] and Alexiou et al. [41] show the strong success in cancer tumor healing by this technique.

Properties of the Ferrofluid

Super paramagnetic behavior is observed in ferrofluid [42]. The direction of the magnetization of the nanoparticles can flip with temperature changes. The time between two direction flips is called the Neel relaxation time [43]. During the absence of external magnetic field, the magnetization of the ferrofluid is relatively low. The Neel relaxation time becomes relatively large during the absence of external magnetic field. This state is called as superparamagnetic state. When an external magnetic field is applied ferrofluid shows behavior similar to paramagnetic behavior. The physical properties of the Ferrotec's EFH1 series educational ferrofluid can be seen in **table 1** below.

Appearance	Black-brown fluid	
Carrier Liquid	Light Hydrocarbon	
-		
-	**CGS Units**	**SI Units**
Saturation Magnetization (Ms)	440 Gauss	44 Mt
Viscosity @27°C	6 Cp	6 mPa·s
Density @25°C	1.21 g/cc	1.21 10^3 kg/m^3
Pour Point	-94 °C	-94 °C
Flash Point	92 °C	92 °C

Table 1- Specifications and physical properties of the ferrofluid which was used in the experiments

Effects on Tuning of a Tank Circuit

Since the ferrofluid contains magnetic nanoparticles in its solution, it can serve as an iron core in our coil. When the ferrofluid flows into the core in response to inlet pressure; the reluctance of the core decreases. Therefore the magnetic field pathway of the coil mostly passes through the ferrofluid and the magnetic field increases. In response to the magnetic field increase, the inductance of the coil increases.

Due to the ferrofluid's fluidity, it is able to flow in response to pressure. The ferrofluid keeps its fluidity under the presence of the magnetic field. Therefore it flows into the core in order to increase the inductance under low pressure.

On the other hand it will leave the core under high inlet pressure and thus the inductance decreases. This is in contrast to other magnetic fluids which are designed to stiffen in the presence of magnetic fields.

2.2 Concept for Direct Control of Rotary Blood Pump Speed by Inlet Pressure

We developed a rotodynamic blood pump speed management technology that results in a pump that responds to inlet pressure in a Starling law-like manner without active electronic controls or pressure sensors. The response is directly to inlet pressure and not based on inferences derived from other signals. **Figure 6** shows the block diagram of the system, and **Figure 7** shows the relationship of the operating frequency and the resonant frequency.

As the inlet pressure drops due to low venous return, ferrofluid flows into coil core volume, inductance increases, and resonant frequency decreases, dropping closer to the operating frequency. The higher tank circuit impedance results in less voltage across the motor and, appropriately, a lower speed. If the inlet pressure increases, ferrofluid leaves the coil volume, resulting in a net increase in resonant frequency and decrease in tank circuit impedance. The motor speeds up to pump the extra blood at the inlet. The flow chart diagrams the series of effects that take place.

As a result the ventricular assist system (VAS) responds to physiologic needs and normal/abnormal transients in a manner very much like the natural heart. The VAS does not depend on reliable residual ventricular function for safety of the speed setting or adequate patient perfusion. A patient could become hypovolemic, agitated, arrhythmic or even experience cardiac arrest, and the control would respond in an effective manner to the blood available at the pump inlet and not to some previous decisions about what the motor current, pump flow or residual pulsatility should be.

Pump performance does not have to deteriorate to the point of detectable abnormalities in the pump current or other parameters in order for the controller to respond, nor the VAS depend on averages determined from a database of prior patients in order to make operative decisions for the one patient in hand.

Patient rehabilitation and quality of life can improve because the VAS responds in a more natural fashion to demands for more or less flow resulting from the patient's activity level, without depending on residual myocardial function or manual adjustments.

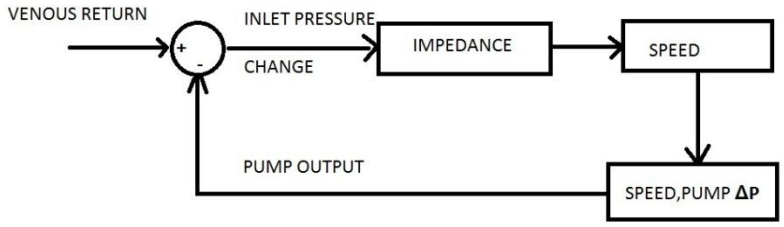

Figure 6 -- illustrates the block diagram of the control system as black-box approach

Venous return and pump output feed into a summer circle and the difference results in an inlet pressure change. The inlet pressure change results in impedance change which causes a speed change. The speed results into a new pump output according to the pump characteristic performance curve. When pump output and venous return equalize, the equilibrium is attained.

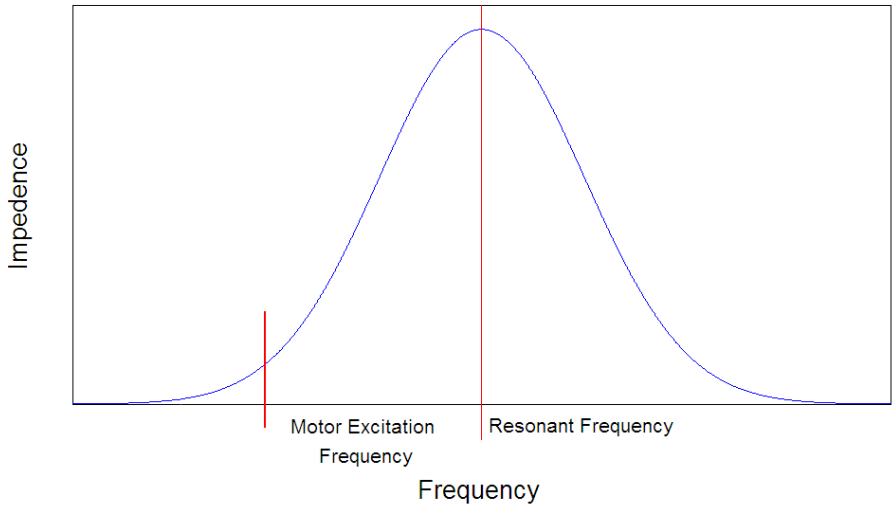

Figure 7 -- shows the ascending and descending part of the tank circuit impendence curve and the operation frequency.

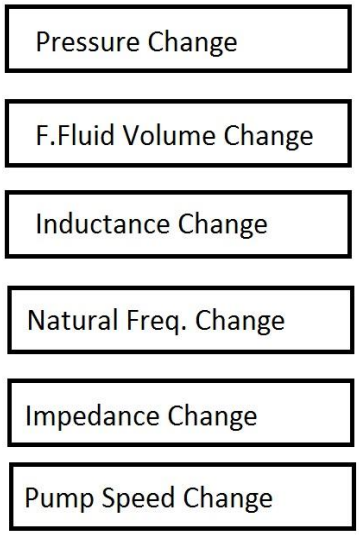

Figure 8 -- The flow chart of the response system.

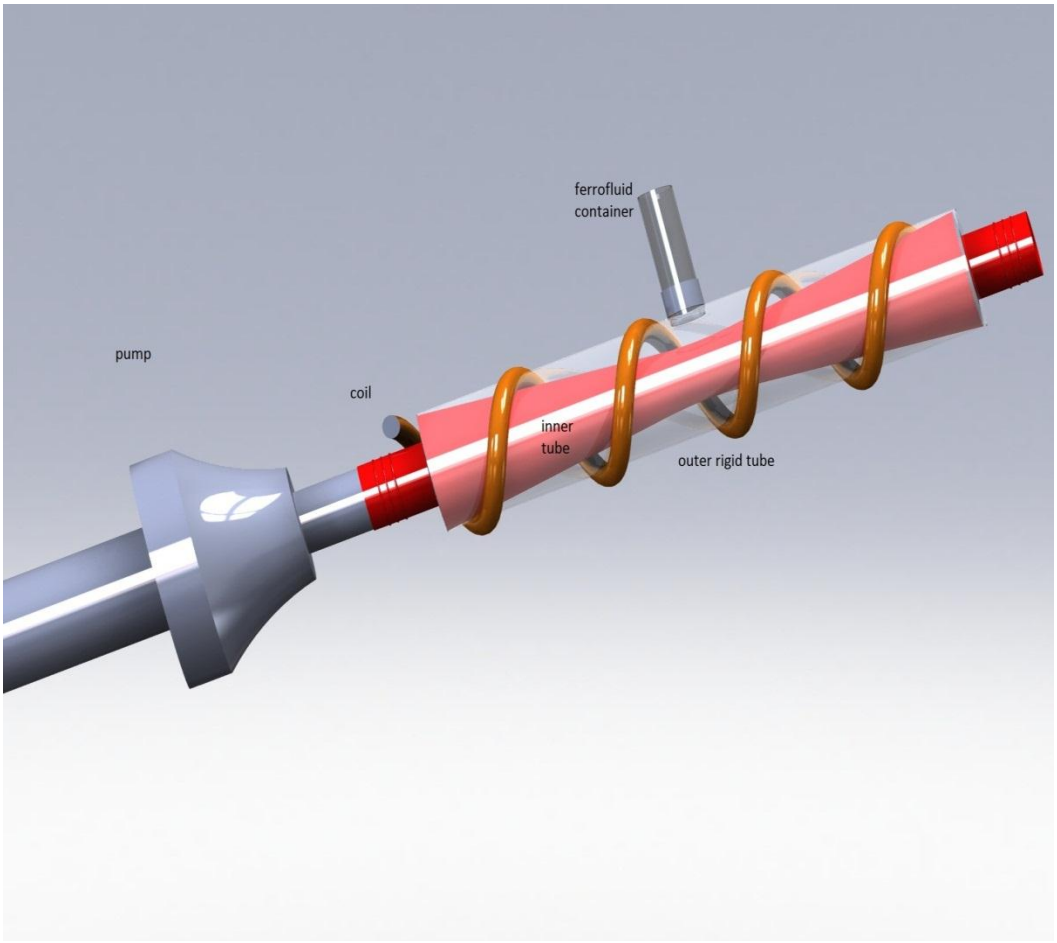

Figure 9 -- Our adjunct electromechanical inlet conduit. The system was designed using Solid Works.

Figure 10 -- The prototype that we developed in house based upon the drawings.

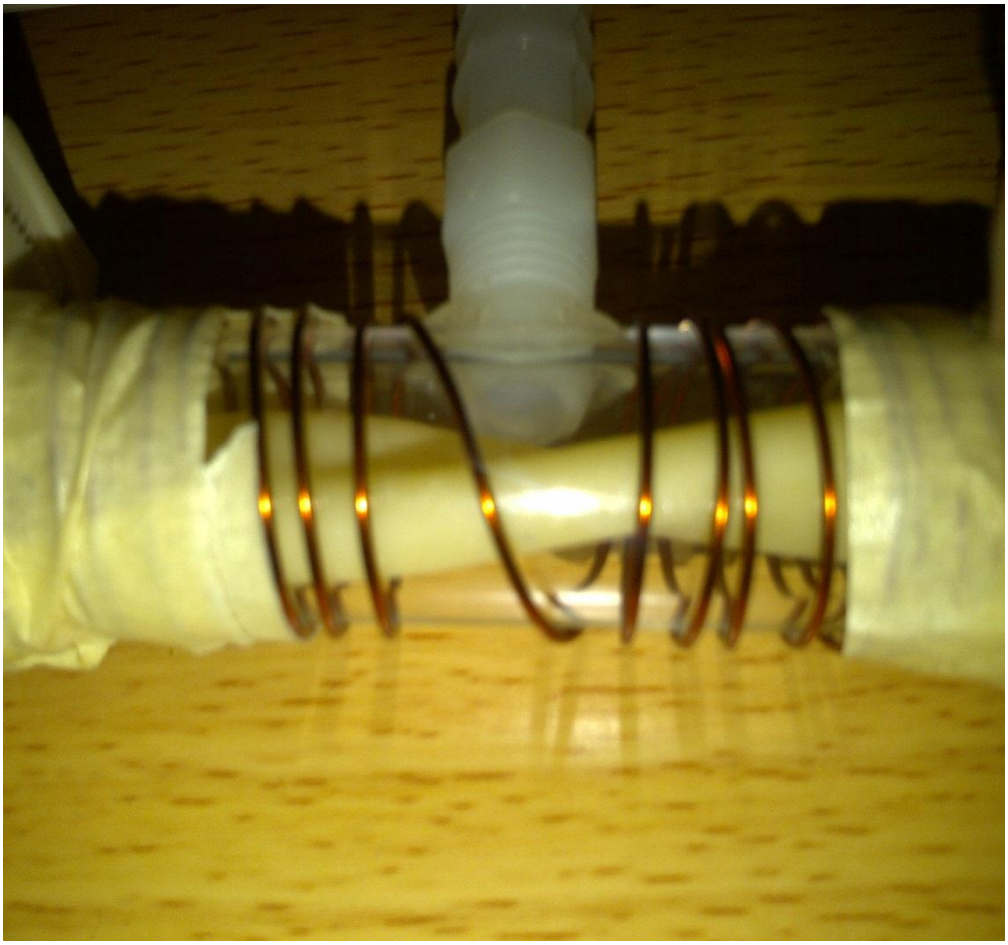

Figure 11 -- A closer look at the inner flexible cylinder which is collapsed with no inlet pressure.

2.3 Long Term Goals and Specific Aims of this Project

The long term goal of the project is to demonstrate a simple, reliable, robust, effective control approach for a rotodynamic ventricular assist device which can simulate a Starling Law flow/pressure response without an active control system and its associated complexities. The design responds to inlet pressure changes without active electronic components or software, and without sensor/control related conductors bulking up the power cable and increasing the risk of conductor fatigue failure.

We had two specific aims in this project:

1) Demonstrate basic feasibility of the concept
2) Begin to define the design issues that will have to be addressed in a more complete study.

2.4 Anticipated Design Issues- Success criteria

A number of tasks/milestones were defined to complete this study:

1) The ferrofluid magnetic performance: Since the ferrofluid is a key component in our system for tuning the tank circuit, we needed to evaluate the ferrofluid properties and behavior within our system and its suitability for the design.
2) Define the frequency: We hypothesized that our system would benefit from a high operating frequency in order to physically minimize the tank circuit components and maximize the "Q" factor. The effects of frequency needed to be explored.
3) Investigate the design of the high frequency power source.
4) Select the side of the tank circuit curve to operate on.
5) Explore the potential interactions and the effectiveness of the tank control circuit concept when it was connected in series with the load.

CHAPTER III

PRELIMINARY TESTING

3.1 Ferrofluid Characterization

A basic unknown which had to be resolved to create a mathematical model of the whole system was magnetic susceptibility of the ferrofluid. By definition magnetic susceptibility of the material ($\mathbf{x}$) equals:

$$\mathbf{x} = \mu + 1 \tag{3}$$

where μ is magnetic permeability of the material.

We used Ferrotec's commercial EFH1 60cc ferrofluid. There are some studies in the literature, which were directed to determine the magnetic susceptibility of the ferrofluid like A. Tari et al. whose goal was to determine the magnetic permeability of the ferrofluid. His research used commercial 200 Gauss ferrofluid containing Fe_3O_4 particles of 7.5 nm diameter in oil host [44].

Equation 4 was used to determine the magnetic permeability of the ferrofluid.

$$\mu = IsV \tag{4}$$

where μ is the magnetic permeability, Is is the magnetization saturation, and V is the volume of the particle. Ferrofluid shows superparamagnetic behavior, while remanence and coercivity was found to be zero [44].

Figure 12 taken from A. Tari et al. showed initial susceptibility of the ferrofluid versus temperature. We are interested in the values around room temperature and body temperature.

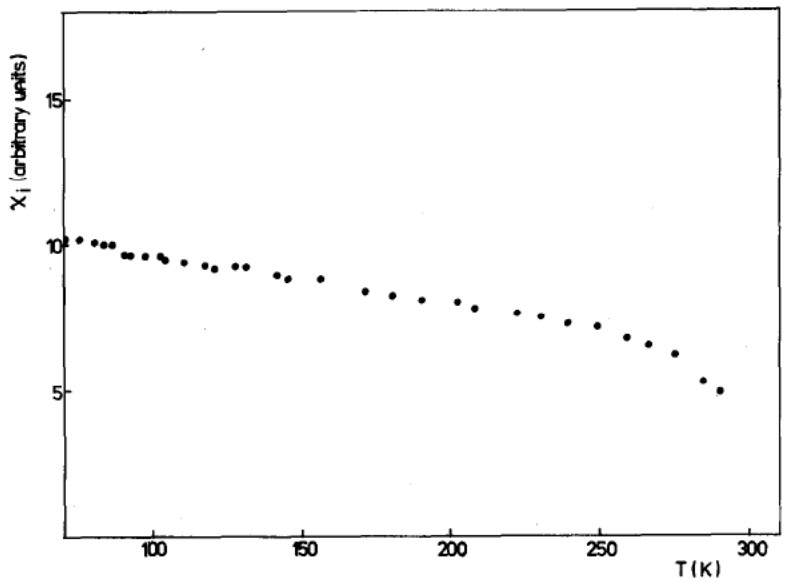

Figure 12 -- The magnetic susceptibility of the ferrofluid curve. Taken from A. Tari et al. [44].

Also, Urtizberea et al. [45] observed the magnetic susceptibility variation of ferrofluid versus ferrofluid's concentration. Since we are using a commercial ferrofluid we are only interested in the magnetic susceptibility of the ferrofluid at the initial concentration. Urtizberea et al. determined the magnetic susceptibility of ferrofluid which they used in their experiments as x=**5.22**. This value is fairly close to the value which was determined by Tari et al. [44]. These two experiments will be the foundation of our experimental design. We took these two studies as references to compare our results.

3.1.1 Test Methods

In order to determine the magnetic permeability of our ferrofluid we developed the following experimental design. We first designed an electronic circuit which included an air gap solenoid coil and resistor connected in series to a coil. The solenoid coil was manufactured in house. We manufactured an air gap solenoid coil wrapped on a plexiglass tube of 0.5 mm wall thickness. Plexiglass is a nonmagnetic material. The diameter of the air gap was 12.7 mm. We then inserted plastic tubing of wall thickness 0.5 mm whose outer diameter was identical to the inner diameter of the solenoid coil. Finally the tubing was filled with ferrofluid. We assumed solenoid coil core was made up of ferrofluid.

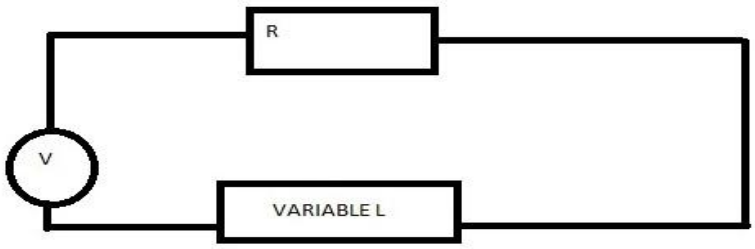

Figure 13 -- The flow chart of the ferrofluid characterization experiment

V and R were initially determined and known.

$$Vr = Vx\frac{zr}{zr+zl} \tag{5}$$

$$Zl = j\omega L \tag{6}$$

$$\omega = 2\pi f \tag{7}$$

After the substitution of the results into those equations, we computed the inductance (L). We used a Wavetek 40 MHz arbitrary waveform generator as a voltage source. We manually adjusted frequencies and amplitude. We applied 10 V p-p sine wave signal from 1 to 20 MHz.

We used equation (8) in order to compute the magnetic permeability.

$$L = \frac{\mu_0\ \mu K N^2 A}{l} \tag{8}$$

where L is inductance, μ_0 is magnetic permeability of air, K is Nagaoka coefficient, A is the crossectional area, and l is the length of the coil. The only unknown was μ. L was computed from our experiment and the other variables were user defined.

3.1.2 Results

The experiment proved to lack conclusive results and we were unable to determine the magnetic permeability of the ferrofluid. We planned to operate at high frequencies but unfortunately the parasitic capacitance of the test inductor was quite high. Therefore the inductor behaved as a capacitor which we had not anticipated. Therefore we were not able to compute the permeability with the ideal magnetic permeability equations.

In addition, due to the nature of the signal generator, the desired voltage value can only be obtained if an internal-external impedance match is provided. Internal impedance of the signal generator was 50 ohms. Since we manually changed the frequency during the experiment to discover the effect of operating frequency change on ferrofluid magnetic permeability, the impedance of the inductor changed which resulted in the value of impedance constantly changing.

We were also unable to deliver full power at all operating frequencies. The applied voltage was differing even though a constant voltage was displayed on the meter screen. Table2 illustrates the results that we got from this experiment.

f(Mhz)	VL	Vr	R	μ
1	4.188	0.5625	1000	0.001174225
2	4.094	2.125	1000	0.000131989
3	4.125	2.812	1000	5.8552E-05
4	4.125	3.031	1000	3.79384E-05
5	4.062	3.25	1000	2.48801E-05
6	4.062	3.406	1000	1.72377E-05
7	4.062	2.25	1000	3.49366E-05
8	4.125	2.875	1000	2.01688E-05
9	4.125	1.969	1000	3.31967E-05
10	4.125	2.781	1000	1.81571E-05
11	4.156	3.094	1000	1.3199E-05
12	4.219	2.062	1000	2.43583E-05
13	4.25	2.469	1000	1.75293E-05
14	4.25	2.969	1000	1.21417E-05
15	4.312	2.281	1000	1.7366E-05
16	4.312	2.594	1000	1.39549E-05
17	4.406	2.969	1000	1.09218E-05
18	4.312	3.156	1000	8.98693E-06
19	4.312	3.438	1000	7.30615E-06
20	4.25	3.625	1000	5.9674E-06

Table 2 -- The results from the ferrofluid characterization experiment

Since we could not determine the exact magnetic permeability with a simple resistor-inductor series connected circuit, we decided to measure inductance of both air gap and ferrofluid filled identical coils. We manufactured a 0.39 μH air gap solenoid coil in house. We inserted a ferrofluid filled experiment tubing (wall thickness = 0.1 mm) whose outside diameter was essentially identical to the solenoid inside diameter into the coil. When we fully inserted the ferrofluid tubing into the coil, we measured the inductance as 0.77 μH. In order to measure the inductance, we used a commercial LCR bridge circuit which has a digital display. After this experiment we simply calculated the magnetic permeability of ferrofluid as 2. The magnetic permeability value does not match the similar experiments that we took as reference. We at least approximated the ferrofluid's effect on coil inductance. The precision of the LCR bridge circuit may have been insufficient, or the low current which is applied by the LCR bridge circuit might be the explanation, because the ferrofluid particles need to be magnetized by an external magnetic field. The magnetization curve of any magnetic material increases until it reaches the saturation point. The current of the measurement device was unlikely to be sufficient to reach the saturation point of the ferrofluid. At least we did demonstrate the effect of the ferrofluid on the core inductance. This characterization experiment became a basis for our mathematical model and the simulations.

3.2 Pedi Pump Electrical Characteristics

In our experiments, we used the Pedi Pump which was developed in the Cleveland Clinic. Pedi Pump is a rotary ventricular assist device that was designed to support the range of patients observed in pediatrics. Pedi Pump uses passive magnetic levitation system. Mixed flow technology was used by the pump impeller, with the flow being accelerated in both axial and radial directions from inlet to outlet. There is also a secondary arterial flow which reenters to the motor gap in order to cool and wash the motor gap. The dimensions of the most recently updated Pedi Pump are 70 mm length and 11 mm diameter [46].

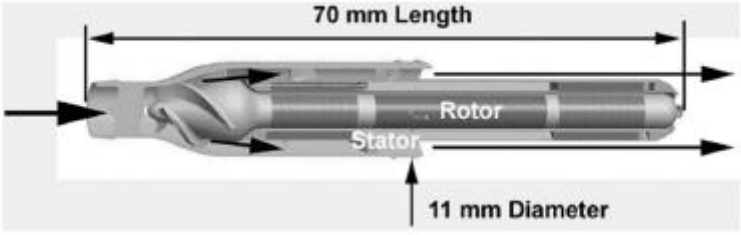

Figure 14 -- The cross sectional view of the Pedi Pump prototype

The Pedi Pump provides from 0.5 liter up to 3 liters flow. The pressure rise range of the pump is from 20 mmHg to over 120 mmHg, depending on speed and applied pressure difference.

3.2.1 Test Methods

In order to get the electrical characteristics of the Pedi Pump we did preliminary mapping. Before the mapping experiment we measured the inductance, capacitance, and resistance of each phase lead. We used an LCR bridge circuit to do these measurements. The inductance in each phase was measured as 43 μH, and resistance was determined to be 3.6 ohms; no parasitic capacitance was detected. The pump was mounted in a steady flow pump mock loop, and the basic overall hydraulic performance determined at 37ºC, using glycerin/water blood analog fluid at a viscosity of 2.5-3.0 centipoise. We used a Brookfield viscometer to document this characteristic. The test loop is a classic "Windkessel" circulation simulation based on the work of Westerhof, Elzinga and Sipkema [47]. We observed the electrical characteristics of the Pedi Pump with various systemic vascular resistances. The systemic vascular resistance was adjusted with a clamp. The clamp was mounted around the main flow tubing and the flow was adjusted to 0, 0.5, 1, 1.5, 2, 2.5, 3 liters per minute. The flow rate was measured by a Transonic flow meter. The flow probe was mounted around the main flow tubing and the ultrasound quality was observed as 93 percent.

The pump was controlled by a console which was developed by The Cleveland Clinic Foundation [48]. The speed of the pump was manually adjusted. The speed was kept constant during the systemic vascular resistance increases. The controller has pump voltage, current, and rpm value displays.

We used a Yokogawa power meter to measure the instantaneous power, current, and voltage readings in the motor leads, thereby avoiding losses associated with the console components. Through this experiment we obtained the current performance of the Pedi Pump in terms of the electrical characteristics.

3.2.2 Results

During this mapping experiment the electrical characteristic readings from the Yokogawa power meter were noted. We obtained the voltage-current-power-impedance data during the pump operation at various speeds and systemic vascular resistances (therefore flow). The figures below illustrate the obtained data. We do not have motor constants for the motor used in the PediPump, so we were not able to calculate the motor terminal voltages and currents at various speeds and loads.

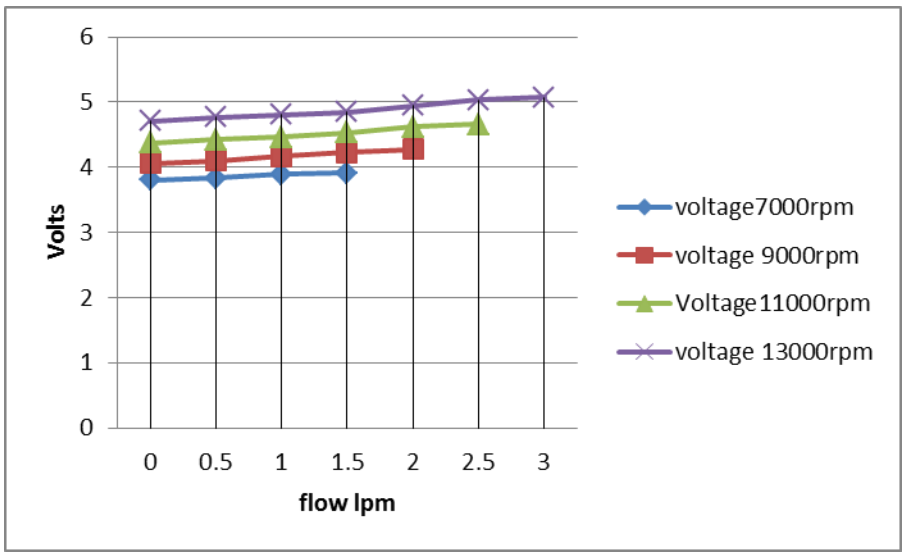

Figure 15 -- The voltage- flow curve obtained with the Yokogawa Power meter

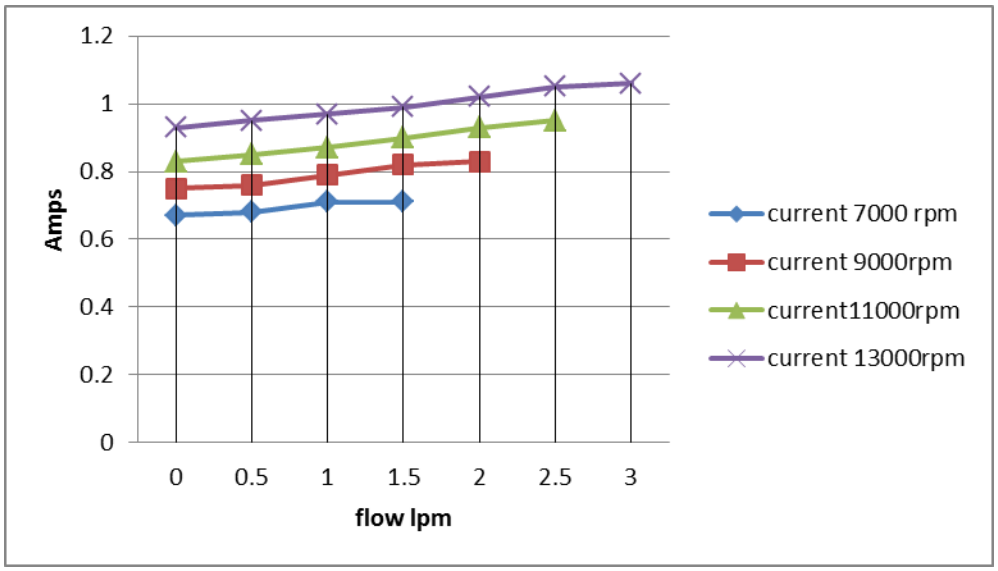

Figure 16 -- The current-flow curve obtained with the Yokogawa Power meter

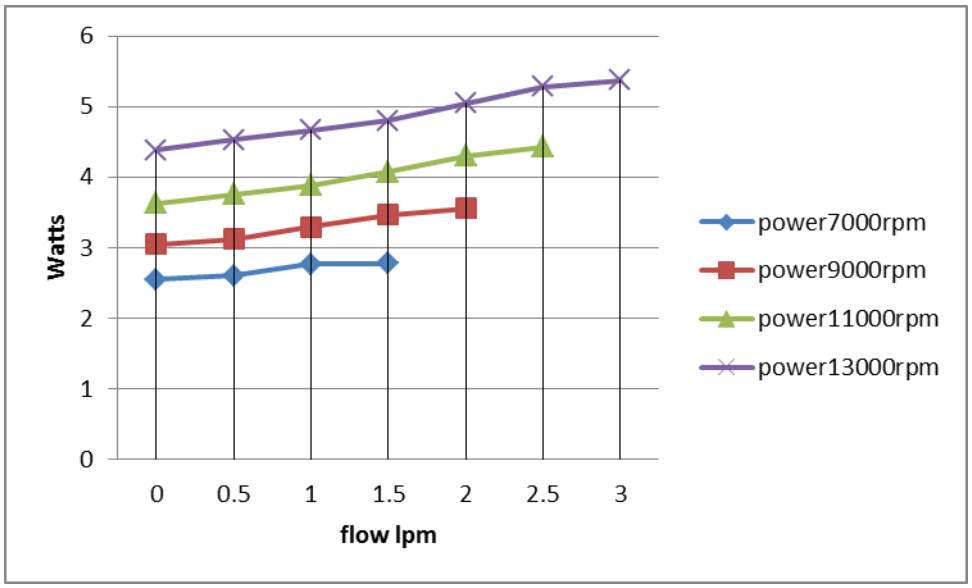

Figure 17 -- The power-flow curve obtained with the Yokogawa Power meter

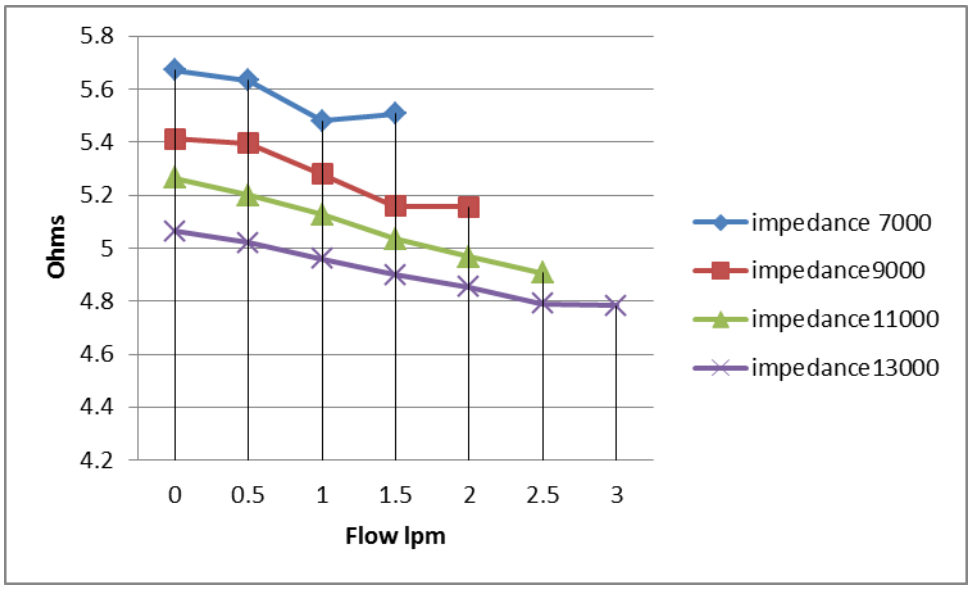

Figure 18 -- The impedance-flow curve derived from the data

3.3 Pedi Pump Open Loop Pressure-Flow-Speed Map

The pressure-flow-speed map of the Pedi Pump was obtained from the same mapping that yielded electrical data. We observed the pressure rise characteristics of the Pedi Pump with various flows and speeds. The systemic vascular resistance was adjusted with a clamp.

The inlet pressures and the outlet pressures were measured using pressure transducers which were mounted to the inlet and the outlet of the Pedi Pump. The pressure readings were amplified through a four channel amplifier in order to get the correct pressure readings. Through this preliminary performance tests we obtained the characteristics of the Pedi Pump. We developed the data which we need to take into consideration while designing our control concept. The basic performance data was applicable in choosing the appropriate components for our concept. The RF amplifier was chosen in order supply adequate power to the motor leads. The performance testing was also useful in choosing the values of the tank circuit components. Figure 19 contains the pressure-flow-speed map of the Pedi Pump that we obtained through our test.

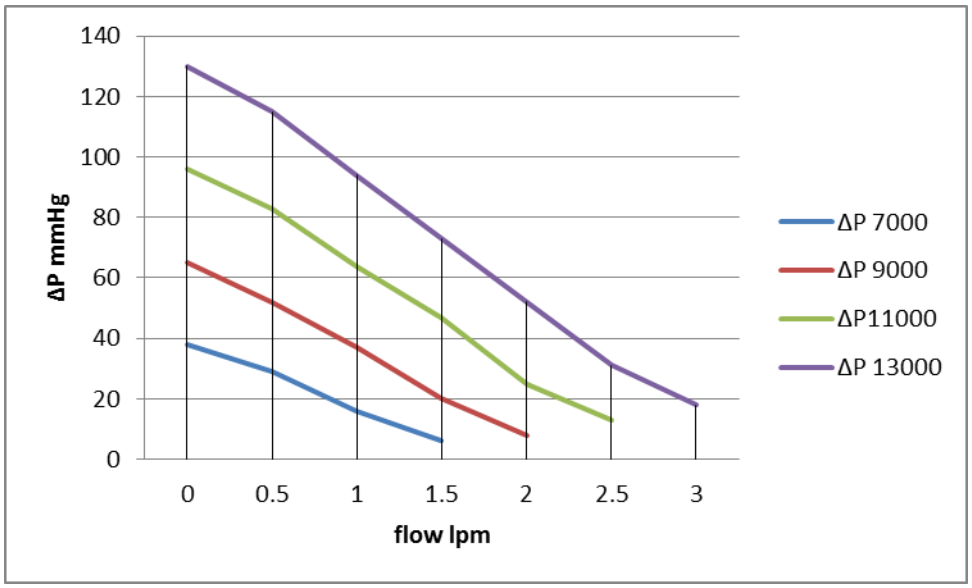

Figure 19 -- The pressure difference-flow curve of the PediPump

3.4 Power Supply Selection

A high frequency (5-20 MHz possible range) power supply capable of 12-20 watts output (to provide a margin over the 6 watts or so to be ultimately delivered to the pump) was a key component of the test system. We found no commercially available hardware operating in this range. Amplifier circuit power amplifier-chips are sold for use in circuits of this type, utilizing current feedback. However, circuit designers told us that it might be a long project to develop a circuit that was stable in operation over a wide range of power outputs, especially since our final frequency and input impedance were not known with certainty at the early stage of the project.

Commercial amateur radio amplifiers had some attractive features, but were designed for higher input and output power levels than we could easily provide as excitation, or use for the pump. Privately designed and built low power amateur radio frequency amplifiers were found at a low price on E-bay that would function with input from a laboratory signal generator, and provide a useful if not perfect output for feasibility studies.

CHAPTER IV

DESIGN ANALYSIS

4.1 Analysis Issues and Approaches

Operating Frequency

In this project, one of the most significant design parameters is the operating frequency. In order to design a highly effective system, we hypothesized that the system should be driven by a high frequency signal.

Since this VAD control system will be incorporated into an implanted package, the control components need to be sufficiently small for the system to be surgically practical. The physical dimensions of the inductor and capacitor become smaller when the operating frequency gets higher. Therefore, the components could be mounted into the pump package. Also, the quality factor (Q factor) gets higher when the system is operated at higher frequency [49]. Traditionally, BLDC motors operate with PWM frequencies above a few tens of kilohertz, so that the motors cannot physically follow the drive oscillation. The voltage is effectively rectified down to DC. Therefore our higher frequencies should be equally acceptable to the motor.

Designing the basic inductor form was based on the size of our test pump. The inner flexible tube had to match the pump inlet diameter and the outer tube diameter and length shouldn't be outlandish compared to the pump. For a starting point, we chose an available tube as the coil form with the following dimensions:

Outer diameter: 1.27 cm

Length: 10 cm

We selected a core which has the same exact dimensions with the experiment tubing in order to eliminate the air effect within the core.

A reasonable number turns to wind by hand were 20. We kept a wide distance between the windings to minimize the parasitic capacitance effect of the inductor and we used 18 AWG wire in order to handle the 2 A current. For these dimensions and the inductance value was 1 µH. The value of an available capacitor was 10 pF and the resulting natural frequency value was 50 MHz. That seemed a good value because our amplifier range was up to 20 MHz and our signal generator has up to 40 MHz signal supply capability. We hypothesized that 10 MHz was a suitable operating frequency in order to start the design process. We simplified the electronic model of our system by eliminating the motor and the driver board. We used a simple pure resistive load in order to represent the pump. We replicated our calculation with 3 different inductance values of 1, 2, and 3 µH in order to represent the hypothesized ferrofluid effect on the tuning.

We developed the mathematical model below:

$$Z_L = J\omega L \tag{6}$$

$$Z_C = \frac{1}{J\omega C} \tag{9}$$

$$Z_X = Z_L // Z_C \tag{10}$$

$$Z_X = \frac{\frac{J\omega L}{J\omega C}}{J\omega C\frac{J\omega L}{J\omega C}+\frac{1}{J\omega C}} \tag{10}$$

$$Z_X = \frac{J\omega L}{1-\omega^2 LC} \tag{10}$$

$$Z_{equal} = \frac{V_{equal}}{I_{equal}} \tag{11}$$

L=1 µH

C=10 pF

V=5 V sine wave

f=10 MHz (empirically selected operating frequency)

$$\omega = 2\pi f$$

$$Z_{equal} = \frac{V_{equal}}{I_{equal}}$$

For L= 1 µH

C= 10 pF

$$Z_{equal} = \frac{j * 2 * 3.14 * 10^{-6} * 10 * 10^{6}}{1 - ((2 * 3.14 * 10 * 10^{6})^{2} * 10^{-6} * 10 * 10^{-12}}$$

Z_{equal} =65.34<90

For L= 2µH

C= 10 pF

$$Z_{equal} = 136.22 < 90$$

For L= 3 µH

C= 10 pF

Z_{equal} = 213.33<90

Theoretically, since we do not have any resistance within the tank circuit (inductor wire eliminated) the angle is always 90^{o} while we operate at the ascending limb (inductive limb). Therefore the impedance increases when the inductance increases. When the inductive effect of the tank circuit becomes equal to the capacitive effect the denominator of equation 10 becomes 0. Therefore mathematically the impedance becomes infinite. When the capacitive effect starts dominating the inductive effect circuit impedance starts decreasing and the angle becomes -90^{0}. That is why the resonance frequency is calculated as:

$$f = \frac{1}{2\pi\sqrt{LC}}$$

Practically this huge instantaneous resonant peak is impossible due to the resistance of the wiring. When we add resistance to the system, we add damping and therefore we smooth the response of the system. Based upon this mathematical model, we simulated our simplified system in Matlab. We expected to obtain different impedance curves for different inductance values. We intended to evaluate the appropriateness of the selected operating frequency or select a better one if the chosen value was inappropriate.

4.2 Impedance Simulation Results

In order to determine the voltage drop across the Pedi Pump, the simplified circuit was simulated. Simulation was done in Matlab/Simulink powersim [50]. Different impedance curves with different inductance values in the tank circuit were obtained with the help of Simulink's applicable PowerGUI. Since the operating frequency is fixed, every impedance curve shift changed the natural frequency/operating frequency relationship. The most linear voltage drop curve was determined. Based upon the ferrofluid characterization experiments we knew that ferrofluid affects the inductance by a factor of 2-3 times. We used these characterization experiments as our reference in order to simulate the inductance change within the simplified model. We preferred the discrete model solution. The step size was 5e-5 for the discrete solution. During the simulation every impedance value which was found by Simulink was saved in the workspace as matrix a matrix row. The simulation was replicated three times and each time we incremented the inductance value within the tank circuit. We obtained three different impedance-frequency curves. We kept the operating frequency constant and matched the obtained curves.

Figure 20– The simplified system Matlab/Simulink model

In the circuit model initial conditions were: L=1 µH and C=10 pF. Capacitance remained constant and inductance was incremented from 1 to 3 µH. After these simulations **figures 21, 22, and 23** below were developed.

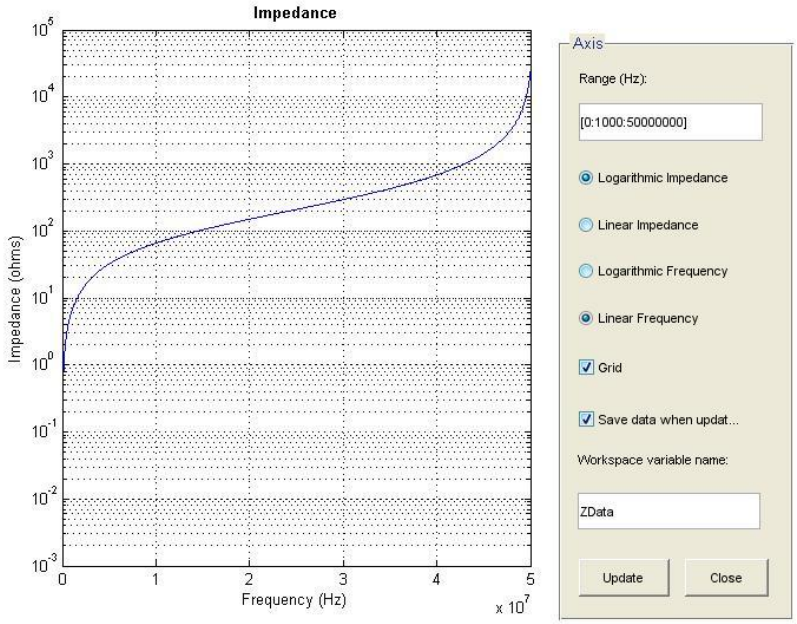

Figure 21 -- The simulation results. The impedance curve of the tank circuit when the inductance = 1µH

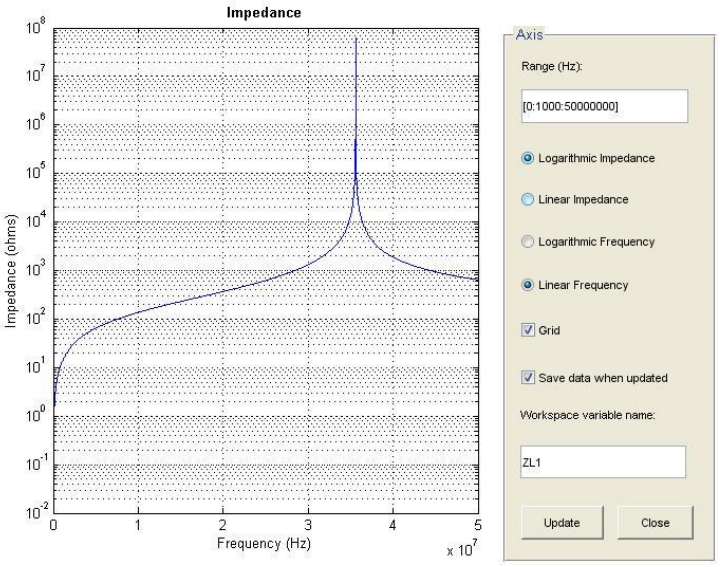

Figure 22 -- The simulation results. The impedance curve of the tank circuit when the inductance = 2µH

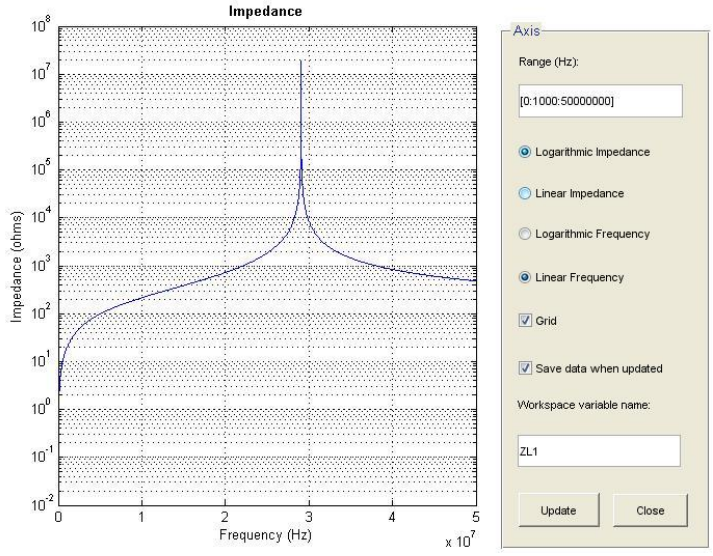

Figure 23 -- The simulation results. The impedance curve of the tank circuit when the inductance = 3µH

Results

During the simulation every impedance value was saved into the Matlab workspace as a matrix row. At the end of the simulation we filtered the impedance values which are obtained for 3 different inductances and 4 different frequencies. Based on these filtered results we had a chance to compare the impedance results at the same operating frequency in order to see the voltage change. Also, we had a chance to see the operating frequency effect in the tank circuit impedance and impedance change as well. T**able 3** shows the impedance values at different inductances and the different operating frequencies.

frequency	Z@L=1 µH	Z@L=2 µH	Z@L=3 µH
1 MHz	j6.28	j12.57	j18.87
5 MHz	j31.72	j64.09	j97.12
10 MHz	j65.41	j136.44	j213.82
15 MHz	j103.44	j292.22	j385.46
20 MHz	j149.2	j367.35	j746.36

Table 3 -- Contains the impedance results at 1, 5,10,15,20 MHz operating frequency and at 1, 2, 3 µH inductance

We wanted to evaluate the suitability of the empirically selected operating frequency within our design. In order to discuss the suitability of the operating frequency, we had two points:

1) A highly linear voltage drop and high impedance difference
2) The lowest possible impedance value during air core operation.

Since the ferrofluid affects the inductance 2-3 times, we did not have a chance to work around a wide range of the curve. Thus, we tried to develop as high impedance change as possible with the low inductance chance. When we checked the obtained results based on the different inductance values 1 MHz operating frequency or even smaller operating frequency are optimum. We took the obtained Pedi Pump impedance characteristic into consideration. While we operated at 1 MHz we had the smallest nominal operation impedance and a fair impedance change in response to inductance change. If we check the higher frequencies like 5 MHz and 10 MHz, we can obviously see that nominal operation impedance is getting high therefore we would not maximize the full speed during operation although the impedance gets higher in response to inductance change. At this point we preferred lower nominal operation impedance and considered 1 MHz as a possible operation frequency.

CHAPTER V

SYSTEM TESTING

5.1 Effect on Tank Circuit Tuning

5.1.1 Methods

After we computed magnetic permeability of the ferrofluid, we set up an experiment to observe the ferrofluid effect in our system. As ferrofluid fills into the coil core, the inductance increases the natural frequency of the tank circuit decreases therefore operating frequency gets closer to the natural frequency, and voltage induced across the Pedi Pump decreases in response to impedance increase of tank circuit. In order to prove this concept we did set up an experimental circuit. **Figure 24** shows the flowchart of the experiment that we set up.

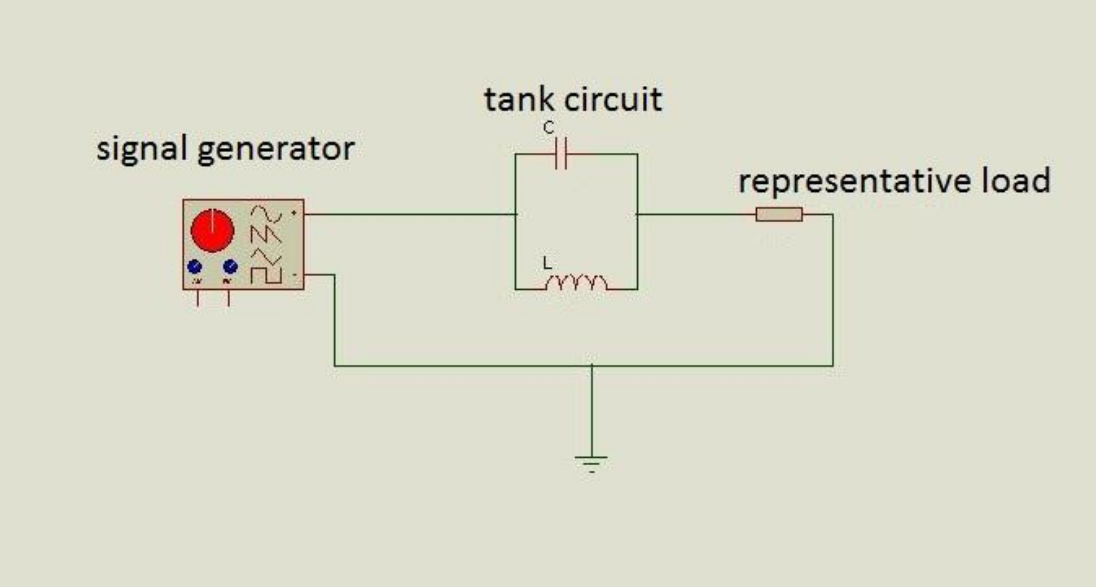

Figure 24 -- The layout of the ferrofluid effect on tank circuit tuning experiment

In this experiment we used a Wavetek 40 MHz arbitrary waveform as the voltage source. We manufactured a 1 µH solenoid air-gap coil as the inductor of the tank circuit.

Capacitance remained constant. The capacitor value was 10 pF. Therefore natural frequency of the tank circuit became 50.3 MHz.

One of the issues which were involved in the experiment was selecting the representative load. Since we did not have a chance to use the pump itself before understanding the behavior of the system we had to use a representative load which was in series with our tank circuit. We decided to use purely resistive load whose value was the exact same (around 5 ohms) value as we obtained through electrical characteristics mapping. We were unable to pick our representative load as 5 ohms.

Since we used a standard signal generator, the internal impedance of the signal generator was 50 ohms. For full power delivery the internal impedance and the external impedance should be matched. Therefore when we used 5 ohm resistor, the supply voltage fluctuated based on the impedance change of the tank circuit in response to inductance change. Thus, we needed to use 50 ohm as the representative load to approximate a value which was around 50 ohms.

The dimensions of the coil that we manufactured in house were:

Inner Diameter R=1.27 cm

Length = 10 cm

The ferrofluid filled experiment tubing had nearly identical dimensions to experiment solenoid coil. We observed the voltage which was induced on the resistor in response to ferrofluid position within the coil.

Operating Frequency Selection: We picked 1 MHz operating frequency based on the data which was obtained through Matlab simulations. Although 1 MHz seemed to work during the simulations, the ferrofluid showed no effect at 1 MHz. We incremented the operating frequency until we got a significant voltage drop. 10 MHz showed the most significant voltage drop range during the experiment. The explanation of why 1 MHz practically did not work as it worked theoretically during the simulation might be the impedance mismatch factor.

Since we had to use 50 ohms as the representative load we could not observe the adequate voltage change. The voltage split between the load and the tank circuit did not adequately change. The load dominated the tank circuit.

5.1.2 Results

The natural frequency of the tank circuit became 35.9 MHz after the ferrofluid tube was fully inserted. The voltage which was measured across the resistor decreased while we inserted the ferrofluid tubing slowly into the coil. We did demonstrate the basic concept through this experiment, before implementing this design into the real inlet conduit concept. **Table 4** and **figure 25** illustrates the results that we obtained.

Position (cm)	Voltage (Volts)
0	7
1	6.9
2	6.8
3	6.7
4	6.5
5	6.3
6	6.1
7	6
8	5.9
9	5.7
10	5.5

Table 4 -- The results of the ferrofluid effect on tank circuit tuning experiment

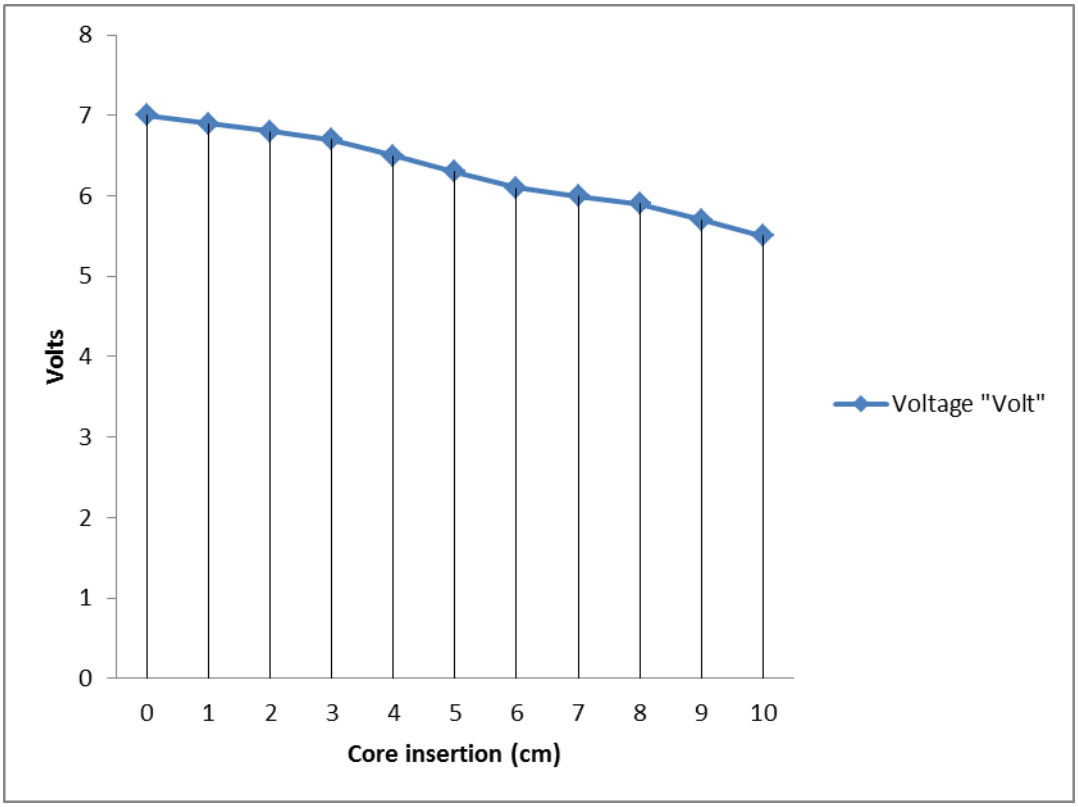

Figure 25 -- The results of the ferrofluid effect on tank circuit tuning experiment. The system was operated at 10 MHz. The voltage drop across the representative load versus ferrofluid experiment tubing position

5.2 Effect on Pump Speed

5.2.1 Methods

We wanted to explore our concept by integrating our manual variable-resonant-frequency tank circuit into the Pedi Pump driving system. In this experiment we used our arbitrary waveform signal generator as the voltage source. Due to the low power of the signal generator we used an RF amplifier to supply adequate power to drive the pump. The tank circuit was fed by the sine wave AC signal from the RF amplifier.

The tank circuit was connected series to the Pedi Pump through the Pedi Pump driver. We aimed to change the speed of the Pedi Pump by changing the natural frequency of the tank circuit in response to ferrofluid quantity within the coil.

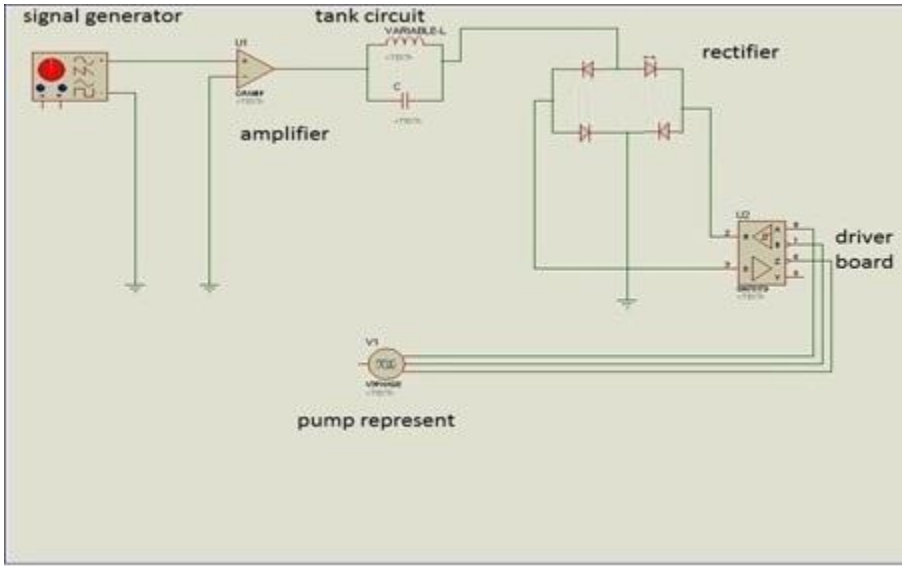

Figure 26 -- The layout of the tuning effect on the Pedi Pump speed experiment

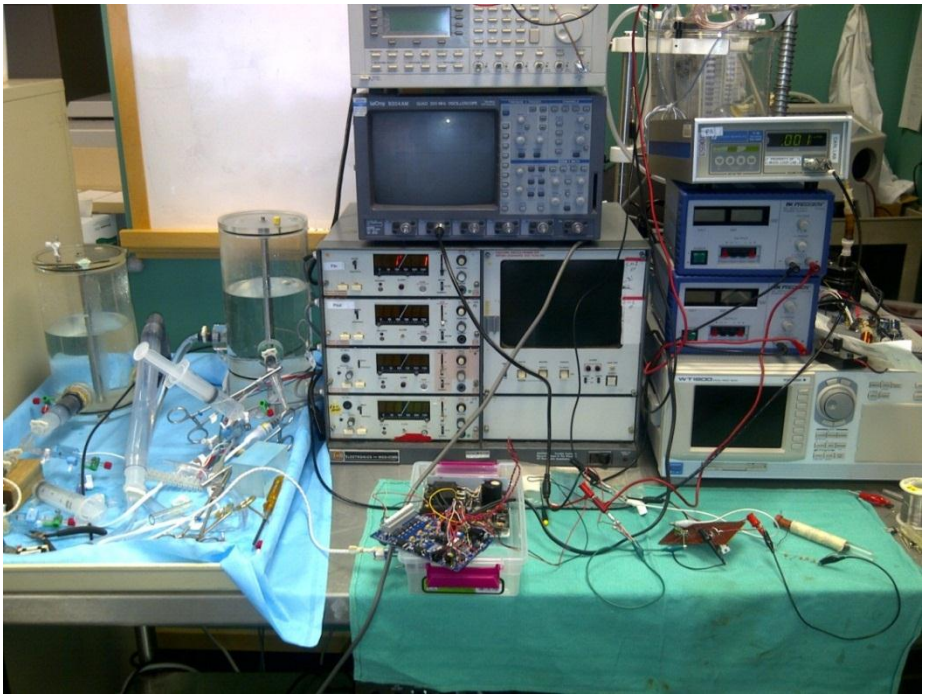

Figure 27 -- The picture of the complete setup

Components

Wavetek 40 MHz arbitrary signal generator and DC power supply

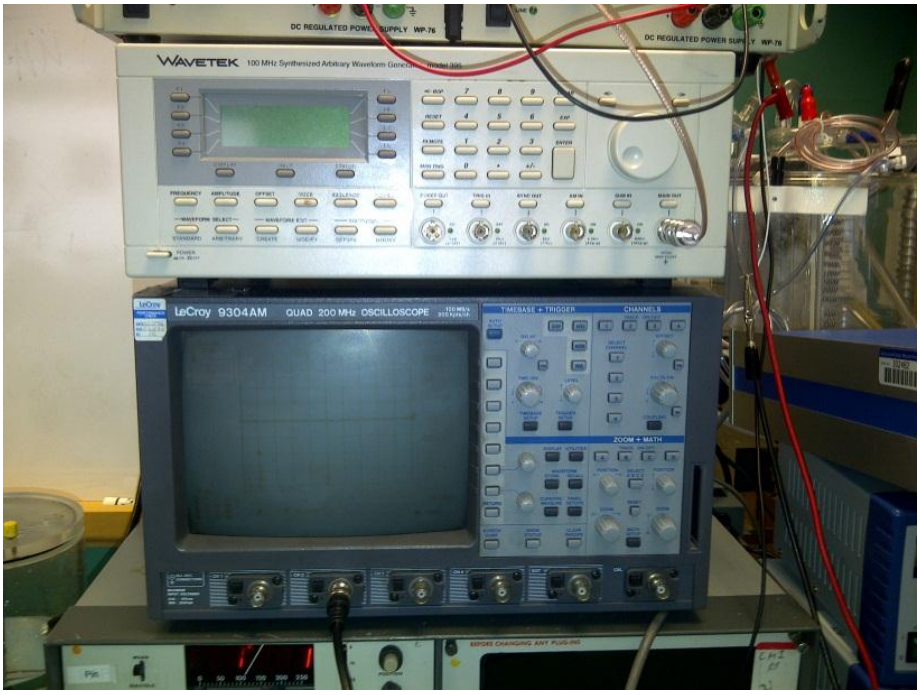

Figure 28 -- The picture of the signal generator and the scope

Tank Circuit

We manufactured another 1 µH inductor. We used 18 AWG wire to increase the current carrying capability of the inductor. We used the same capacitor that we used in basic tank circuit experiment. The natural frequency of the tank circuit that we set up was 50.3 MHz without ferrofluid insertion to the core. We used the same ferrofluid tubing to insert to the core. The dimensions of both tubing and core weren't changed. The natural frequency of the tank circuit became 35.9 MHz after the ferrofluid tubing was fully inserted.

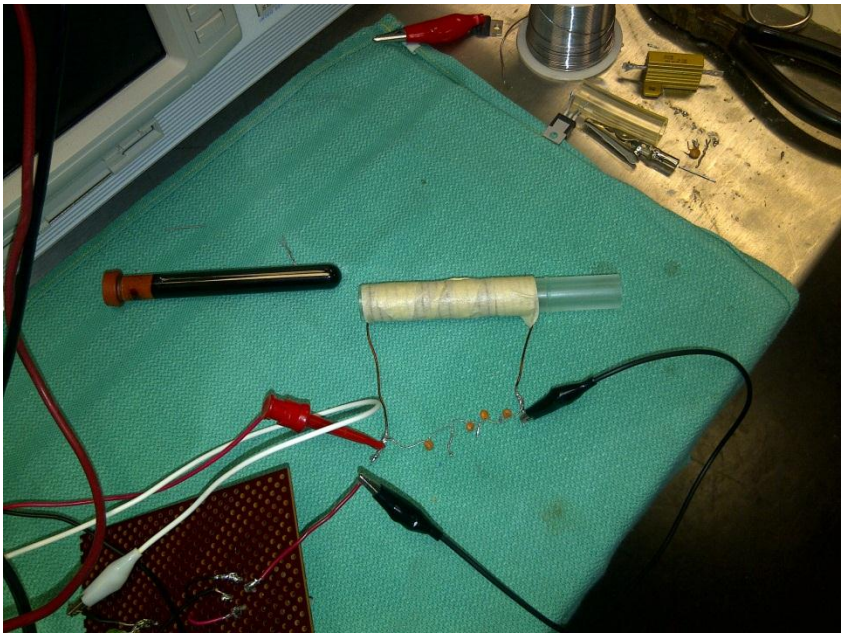

Figure 29 -- The picture of the 1 µH air core coil and the experiment tubing which is filled with ferrofluid

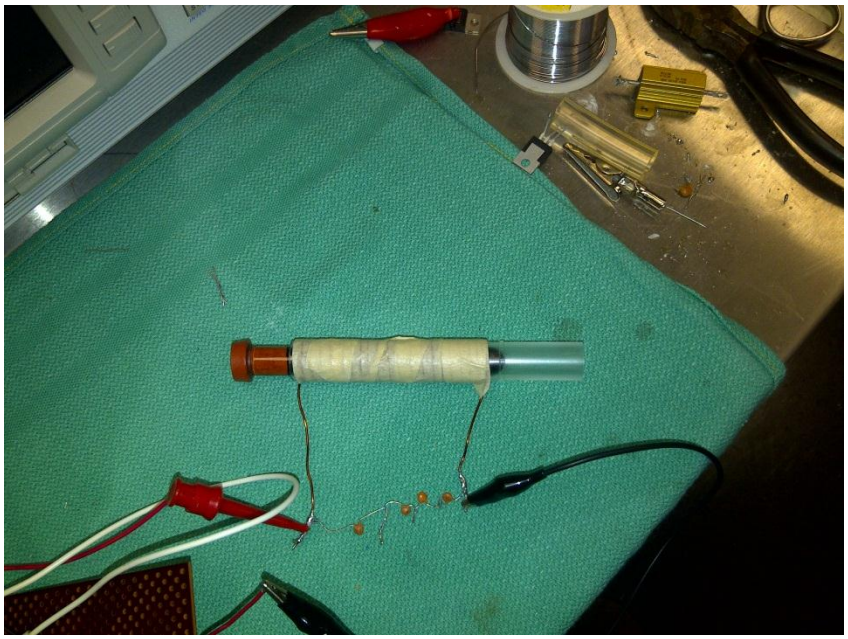

Figure 30 -- The picture of the ferrofluid tubing while inserted into the air core coil

Rectifier

We did not plan to rectify the current after the tank circuit. However the brushless DC motor driver board in the console would not function with 10 MHz. signals routed through its transistors. We hypothesize that the transistors shorted through internal parasitic capacitances at this frequency almost two orders of magnitude higher than the intended motor excitation frequency.

Schottky diodes

Schottky diodes are made with metal to n junction rather than P-N junction conventional diodes. This feature provides very lower reverse recovery time than conventional diodes and lower voltage drop as well. Schottky diodes are highly preferred for high frequency applications.

Rectifier circuit

In order to find appropriate diodes, we had two constraints. The reverse recovery time was our one of the constraints due to high frequency. Since we were operating 10 MHz the appropriate reverse recovery time was calculated. Since the natural characteristic of the AC signal the half of the period was positive and the other half of the period was negative. We were interested in rectifying the negative half into positive. Therefore we considered two halves as separate periods and the signal frequency was considered as 20 MHz.

We considered the Nyquist approach [51] in order to prevent the aliasing occurrence within rectification process. Therefore the reverse recovery frequency should be higher than 40 MHz. Thus the appropriate reverse recovery time was smaller than 25e-12 seconds. We bought the appropriate rectifier diodes from the market. We applied full-wave bridge rectification to the ac signal which was coming through the tank circuit. We used filter capacitors to prevent the triple peaks within the signal.

Therefore we had DC voltage in order to feed the pump through the gate transistors of the motor driver. The amplitude of the DC voltage showed the same amplitude variability as AC signal in response to ferrofluid tubing insertion to the core.

The second constraint of the rectification was the output current capability of the diodes. Since we need up to 2 amps current the diodes we used was supposed to be capable of providing up to 2 amps. The diodes that we purchased were capable of providing up to 8 amps.

On the other hand, the threshold voltage of the diodes was the factor that we needed to be careful as well. Through the characteristic nature of the Schottky diodes we did not have to worry about the power loss during rectification.

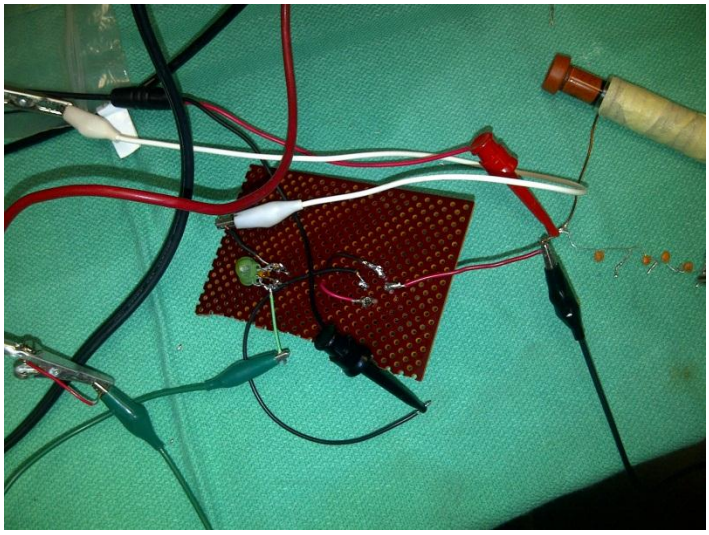

Figure 31 -- The picture of the full bridge rectifier circuit which is connected to the tank circuit

PICDEMLV Brushless DC Motor Driver

The pump was operated using a PICDEM MC LV Development motor driver board from Microchip Technology Inc. (Chandler, AZ). This board has an advantage for us that the electronic supply and the motor bridge supply can be separated. Through this feature the chip was fed by constant DC and motor bridges were fed by variable amplitude DC which came through our control circuit.

Mock Loop

In order to test our system, we needed to test the Pedi Pump speed change in response to ferrofluid position in the core. We did set up a mock circulatory system. We used PVC tubing in order to represent vessels within the human body.

In order to represent blood flow, we used water-glycerin mixture. The viscosity of the water-glycerin mixture was adjusted as 2.5-3 centipoises. We integrated the Pedi Pump into the mock loop. We observed the pump speed by observing the flow rate. The flow rate was measured by a Transonic Flow meter. We observed the flow-rate in response to ferrofluid tubing position within the core.

5.2.2 Results

We did set up all the components of the experiment and the control circuit that we designed. We connected the Pedi Pump in series to tank circuit through the transistors of the motor driver board. Therefore the amplitude of the voltage across the Pedi Pump changed in response to ferrofluid position within the coil response to natural frequency shift of the tank circuit. Therefore the flow rate changed in response to voltage change across the Pedi Pump. **Figure 32** shows the obtained results from this experiment.

Position (cm)	Flow (liters/minute)
0	2
1	1.8
2	1.7
3	1.6
4	1.4
5	1.3
6	1.2
7	1.1
8	1.05
9	1
10	1

Table 5 -- The results which were obtained from the effect of tuning on the Pedi Pump speed experiment. The flow decreased in response to ferrofluid tubing insertion into the air core coil

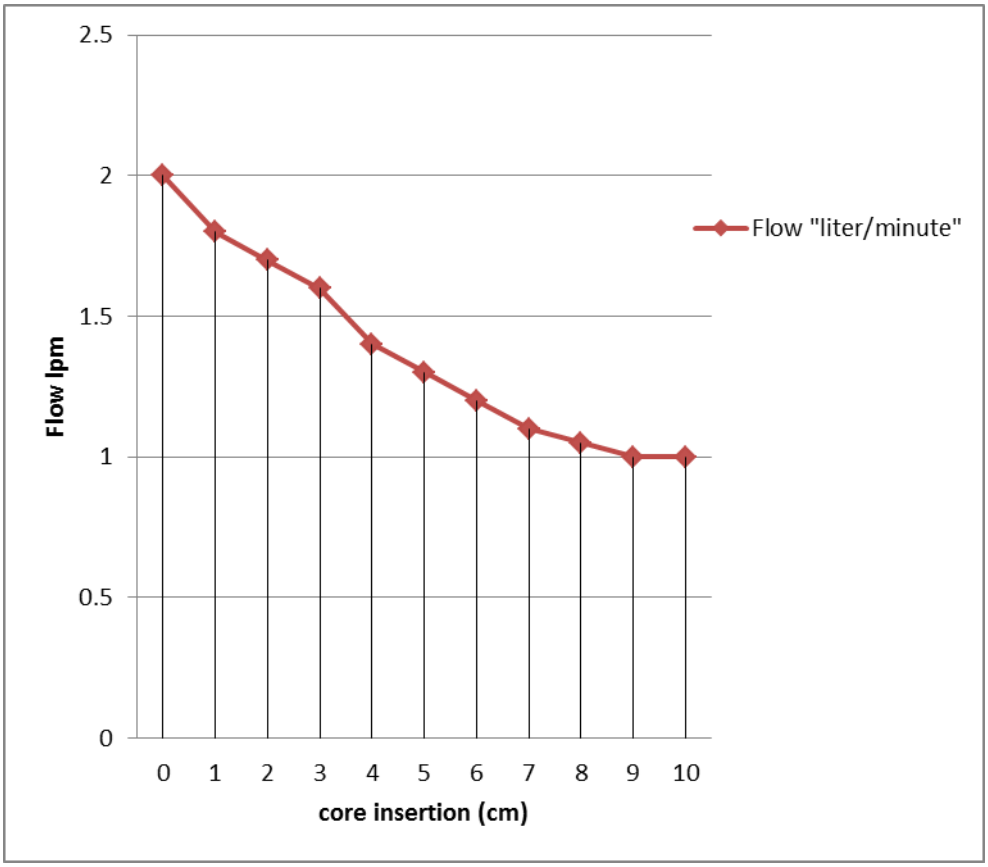

Figure 32 -- The data from the experiment. The system was operated at 10 MHz. The speed decrease is linear with the core insertion

5.3 Ongoing Tests

Following the proof of the concept, we started testing our inlet conduit prototype. The inlet conduit prototype was built by hand based on the Solid Works drawings. A Penrose drain was used as the inner flexible cylinder. We folded the two edges of the inner flexible tube over to the outer cylinder and we clamped both of them for sealing purposes. We drilled the outer cylinder through its surface and attached tubing as the ferrofluid reservoir. The outer cylinder dimensions and material were identical to the coil that we built for experiment tubing insertion experiments. We wound 20 turns wire to the inductor and used same capacitor in order to get the identical tank circuit that we were already familiar We integrated this prototype into the Mock Loop. The Mock Loop properties were kept identical to the previous experiments. We used same pressure transducers and four channel amplifier to measure the input and output pressures of the Pump.

We used an adjustable air pressure source in order to maintain the inlet pressure constant.

We had many mechanical obstacles as described below.

Leakage: Ferrofluid leaked out of its designated space which is between inner and outer cylinder. Ferrofluid leaked into the water-glycerin mixture and pump.

Inner flexible tube: The inner flexible tube did not expand enough and did not collapse completely as desired. It sometimes closed the ferrofluid reservoir orifice and prevented the ferrofluid in-out flow. We still do not have a fully functional and sealed mechanical prototype to test. A more promising design, based on an intra-aortic balloon pump membrane is being constructed as this thesis is written.

CHAPTER VI

CONCLUSION AND RECOMMENDATIONS

6.1 Discussion of the Results

A fundamental goal of this project was a proof of concept demonstration, and we did show most of the functions required by the concept. The second goal was to develop an understanding of these issues to be addressed to go further with the control approach and we did develop significant data in this area.

Ferrofluid effect on tuning experiment

During the simple ferrofluid effect on the tank circuit tuning experiment, a 50 ohm resistor was used to represent the Pedi Pump. Since the impedance of the Pedi Pump was estimated to be of the order of 5 ohms during the operation, this load representation was not realistic. First of all, Pedi Pump cannot be considered as a purely resistive load due to the existence of the inductive load on the PediPump. We were obligated to use a 50 ohms load because the available power supply equipment was impedance matched in this range. We could not optimize the tank circuit nominal operation impedance and it was higher than desired impedance value.

Also there is an unexplained inconsistency between the simulations and the practical experiments. The Matlab simulations indicated that 1 MHz or even lower would be the optimum operating frequency, the practical experiments showed that 10 MHz as the workable operating frequency. This difference cannot be accepted as a measurement error in practical study.

Since we used a bigger load to impedance match the signal generator, the voltage difference across the tank circuit became small and difficult to measure. If we could employ a smaller resistor on the order of 5-10 ohms the voltage split between the tank circuit and the resistor will be more favorable and the voltage drop will be visible. Since we had to match the impedances we did not have a chance to use smaller load for the representation.

Control Concept Effect on Pump Speed

The compromises of the first experiment affected our tank circuit effect on pump speed change experiment. The Pedi Pump is able to provide up to 3 liters per minute flow. However the maximum flow we observed was 2 liters per minute. The reasons why we could not observe 3 liters per minute as the maximum flow can be categorized into two groups and also these two groups are related each other.

High nominal impedance of the tank circuit

Since we compromised while we were selecting the optimum values of the tank circuit, the nominal operation impedance of the tank circuit was much higher than the Pedi Pump. When we increased the inductance by inserting our ferrofluid tubing, the impedance of our tank circuit became higher still. Tank circuit voltage drop was excessive.

Amplifier

Because of the impedance mismatch which became greater as the ferrofluid content in the core became greater, our amplifier was inefficient and overloaded at many operating conditions. It could not always output adequate voltage. Its output was not stable as it overheated.

Ferrofluid

We used EFH1 series of ferrofluid manufactured by Ferrotec Corp, which was available at the Cleveland Clinic. This ferrofluid is manufactured for educational demonstration, and has a low magnetic permeability, low magnetic saturation and low viscosity. Since we dealt with a ferrofluid which has a low magnetic permeability we get the maximum possible impedance range for a wide speed range. The company's EMG 900 series ferrofluid seems promising for this concept. With EMG 900 type ferrofluid, we expect four times inductance change which will provide significantly more inductance change. Through this inductance change we will be more successful in duplicating Frank-Starling law behavior.

On the other hand, we are still not confident about our understanding of the ferrofluid magnetic behavior as a core material. Since we were unable to exactly determine the magnetic properties of ferrofluid, we still do not know how it behaves as a core material. As all magnetic materials, ferrofluid has different magnetization values under the existence of the different magnetic field until it reaches to the saturation. Since the Pedi Pump has different power levels at different RPMs and different ΔP values, we still do not know if the magnetic properties of the ferrofluid are stable or not under these different circumstances. Due to the lack of laboratory equipment to determine and record the magnetic properties of the ferrofluid, it is currently remaining as an unknown.

Rectifier

In our conceptual design, we were not planning to rectify the AC voltage. We aimed to drive the motor directly by the AC power through the driver board. We shifted our AC signal up through a high frequency operational amplifier by adding a bias dc voltage. The amplitude of the signal varied from 0 to 10 V P-P. The incapability of the driver in handling high frequency did not let us to run the Pedi Pump. Therefore, we had to integrate a rectifier between the tank circuit and the driver board. Thus, AC power was rectified to DC power, and went through the driver as a variable amplitude DC power.

6.2 Conclusion and Future Work

The variable inductor, tank circuit concept clearly can be used to make the pump speed vary, without using components of outlandish physical size or electrical characteristics. In order to pursue this study and manufacture an implantable pump package prototype there are a number of tasks which need to be accomplished.

We need a high frequency power supply that is efficient working into the range of input impedances desired for this control concept. This is not easily found commercially, and may be a somewhat sophisticated design challenge for an engineer experienced with radiofrequency circuits. Reliable stability is the issue raised by the Cleveland Clinic's circuit designer. The motor commutation transistors must have the ability to pass radio frequencies. The low end impedance of the tank circuit must be closer to zero, to permit full speed operation of the pump with little voltage drop in the tank circuit.

This is a matter of further optimizing tank circuit design and operating frequency choice. The inductance variation should be increased, to increase the range of speed. Much higher magnetic permeability ferrofluids are made, and would enable this design feature. We need a better understanding of the magnetic properties of the ferrofluid as a function of frequency and current.

The most immediate next task is to test with the prototype inlet conduit that has been built, using an intra-aortic balloon pump membrane as the flexing inner element. This will be direct demonstration of the speed control by inlet pressure, and will also explore the ability of the concept to maintain normal blood pump pressures, rather than to damp them as is the case with current rotodynamic blood pump implants.

The Yokagawa power analysis instrument can probably be used to determine circulating currents in the tank circuit, which will be an important characteristic to track to minimize real power losses in the tank circuit.

The practicality of incorporating a tank circuit in each motor lead, close to the pump, is yet to be evaluated. This would eliminate leads carrying the inductor value back to the console, but will put two tank circuits in series with each working coil. The back-emf will also have to traverse a tank circuit, but the back-emf frequency is relatively low so that only losses in the presumably low coil resistance should be a factor.

With this experience, we will be in a position to design a first prototype product of size, durability, and electrical performance suitable for implant use.

BIBLIOGRAPHY

1. *Rosamund W, et al. Heart Disease and Stroke Statistics—2008 Update* Circulation.*117:e25*e146, 2008.
2. Hogness JR and Van Antwerp M, et al. The Artificial Heart - Prototypes, Policies and Patients. National Academy Press, Washington D.C. 1991.
3. Willman, VL., chair. Expert Panel Review of the NHLBI Total Artificial Heart Program June 1998-November 1999 http://www.nhlbi.nih.gov/resources/docs/tah-rpt.htm (accessed 3 August 2009)
4. Delgado, R., and Bergheim, M. 2005. HeartMate II left ventricular assist device: a new device for advanced heart failure. *Expert Rev Med Devices* 2:529-532.
5. Griffith, B.P., Kormos, R.L., Borovetz, H.S., Litwak, K., Antaki, J.F., Poirier, V.L., and Butler, K.C. 2001. HeartMate II left ventricular assist system: from concept to first clinical use. *Ann Thorac Surg* 71:S116-120; discussion S114-116.
6. El-Banayosy, A., Arusoglu, L., Kizner, L., Morshuis, M., Sarnowski, P., Cobaugh, D., and Koerfer, R. 2006. Performance of the CorAide LVAS in potential destination therapy patients. *Asaio J* 52:51A.
7. Esmore, D.S., Kaye, D., Salamonsen, R., Buckland, M., Rowland, M., Negri, J., Rowley, Y., Woodard, J., Begg, J.R., Ayre, P., et al. 2005. First clinical implant of the VentrAssist left ventricular assist system as destination therapy for end-stage heart failure. *J Heart Lung Transplant* 24:1150-1154.

8. http://www.circulite.net/our_technology/our_clinical_trials, Proof of Concept: Hemodynamic Response to Long Term Partial Ventricular Support with the Synergy™ Micro-pump, 2009, abstract Presented at the 58th Annual Scientific Session of the American College of Cardiology.
9. Ochiai, Y., Golding, L.A., Massiello, A.L., Medvedev, A.L., Horvath, D.J., Gerhart, R.L., Chen, J.F., Krogulecki, A.Y., Takagaki, M., Doi, K., et al. 2002. Cleveland clinic CorAide blood pump circulatory support without anticoagulation. *Asaio J* 48:249-252.
10. Xu, L., Wang, F., Fu, M., Medvedev, A., Smith, W.A., and Golding, L.A. 1997. Analysis of a new PM motor design for a rotary dynamic blood Pump. *Asaio J* 43:M559-564.
11. Sweeney, M.S. 1999. The Hemopump in 1997: a clinical, political, and marketing evolution. *Ann Thorac Surg* 68:761-763.
12. Garatti, A., Colombo, T., Russo, C., Lanfranconi, M., Milazzo, F., Catena, E., Bruschi, G., Frigerio, M., and Vitali, E. 2005. Different applications for left ventricular mechanical support with the Impella Recover 100 microaxial blood pump. *J Heart Lung Transplant* 24:481-485.
13. Siess, T., Nix, C., and Menzler, F. 2001. From a lab type to a product: a retrospective view on Impella's assist technology. *Artif Organs* 25:414-421.
14. http://www.fda.gov/cdrh/pdf6/K063723.pdf

15. Schmid, C., Tjan, T.D., Etz, C., Schmidt, C., Wenzelburger, F., Wilhelm, M., Rothenburger, M., Drees, G., and Scheld, H.H. 2005. First clinical experience with the Incor left ventricular assist device. *J Heart Lung Transplant* 24:1188-1194.
16. Takatani, S., Matsuda, H., Hanatani, A., Nojiri, C., Yamazaki, K., Motomura, T., Ohuchi, K., Sakamoto, T., and Yamane, T. 2005. Mechanical circulatory support devices (MCSD) in Japan: current status and future directions. *J Artif Organs* 8:13-27.
17. De Robertis, F., Birks, E.J., Rogers, P., Dreyfus, G., Pepper, J.R., and Khaghani, A. 2006. Clinical performance with the Levitronix Centrimag short-term ventricular assist device. *J Heart Lung Transplant* 25:181-186.
18. Guyton, Arthur C., and John E. Hall. *Textbook of Medical Physiology*. Philadelphia: Elsevier Saunders, 2006.
19. Samuels L. Biventricular mechanical replacement. *Surgical Clinics of North America.* 84(1):309-21, 2004.
20. Cooper DS. Jacobs JP. Moore L. Stock A. Gaynor JW. Chancy T. Parpard M. Griffin DA. Owens T. Checchia PA. Thiagarajan RR. Spray TL. Ravishankar C. Cardiac extracorporeal life support: state of the art in 2007. *Cardiology in the Young.* 17 Suppl 2:104-15, 2007

21. Wieselthaler GM, Schima H, Dworschak M, et al. First experiences with outpatient care of patients with implanted axial flow pumps. *Artif Organs* 2001;25:331–5.
22. Vollkron M, Voitl P, Ta J Wieselthaler G, Schima H. Suction events during left ventricular support and ventricular arrhythmias *J Heart Lung Transplant* 2007;26:819–25
23. Vollkron M, Schima H, Huber L, Benkowski R, Morello G, Wieselthaler G. Advanced suction detection for an axial flow pump *Artificial Organs* 30(9):665–670, 2006.
24. Bullister E, Reich S, Sluetz J. Physiologic control algorithms for rotary blood pumps using pressure sensor input. *ArtifOrgans* 2002;26:931–8.
25. Yamagishi H, Sankai Y, Yamane T, Jikuya T, Tsutsui T. Development of built-in type and noninvasive sensor systems for smart artificial heart. *ASAIO J* 2003;49:265–70.
26. Wilhelm, M.J., Hammel, D., Schmid, C., Stypmann, J., Asfour, B., Kemper, D., Schmidt, C., Morley, D., Noon, G.P., Debakey, M.E., et al. 2001. Clinical experience with nine patients supported by the continuous flow Debakey VAD. *Journal of Heart Lung Transplantation* 20:201.
27. Choi S. Boston JR. Antaki JF. Hemodynamic controller for left ventricular assist device based on pulsatility ratio. *Artificial Organs.* 31(2):114-25, 2007.

28. Nakata KI, Yoshikawa M, Takano T, et al. Control system for an implantable rotary blood pump. *Ann Thorac Cardiovasc Surg* 2000;6:242–6
29. Konishi H, Antaki JF, Amin DV, Boston JR, Kerrigan JP, Mandarino WA, Litwak P, Yamazaki K, Macha M, Butler KC, Borovetz HS, Kormos RL, Controller for an axial flow blood pump. *Artificial Organs*. 20(6):618-20, 1996
30. Vollkron M, Schima H, Huber L, Benkowski R, Morello G, Wieselthaler G. Advanced suction detection for an axial flow pump *Artificial Organs* 30(9):665–670, 2006.
31. Patrick, Dale R., and Stephen W. Fardo*. Rotating Electrical Machines and Power Systems*. Lilburn, GA: Fairmont, 1997.
32. Krishnan, R. "PM Brushless DC Machine." *Permanent Magnet Synchronous and Brushless DC Motor Drives*. Boca Raton: CRC/Taylor & Francis, 2010.
33. *Motion Control Engineering Handbook.* Sub-Title: DC (Direct Current) Servo Motors /Tachometers / Brushless DC). (Canoga Park, Calif.): Magnetic Technology, 1985.
34. Brushless DC Motors Handbook. http://www.axsys.com/documents/Brushless_DC_Motors.pdf
35. Horowitz, Paul, and Winfield Hill. *The Art of Electronics*. Cambridge [England: Cambridge UP, 1989.
36. S. S. Papell, U.S. Patent no :3, 215, 572 (1965)

37. Scherer, C. *Ferrofluids: Properties and Applications.* Brazilian Journal of Physics. 30(5),2005.

38. R. Moskowitz and R. E. Rosensweig, Appl. Phys. Lett. 11,301 (1967).

39. http://ferrofluid.ferrotec.com/ferrofluid-home/

40. A. S. Lübbe, C. Alexiou, and C. Bergemann, "Clinical Applications of Magnetic Drug Targeting", *Journal of Surgical Research* 95, 200 (2001)

41. Ch. Alexiou, R. Schmid, R. Jurgons, Ch. Bergemann, W. Arnold and F.G. Parak, Targeted Tumor Therapy with Magnetic Drug Targeting: Therapeutic Efficacy of Ferrofluid Bound Mitoxantrone, in Ferrofluids: *Magnetically Controllable Fluids and Their Applications*, Ed. Stefan Odenbach, Springer,2002, pg 233;

42. Moeser, Geoffrey D. *Colloidal Magnetic Fluids as Extractants for Chemical Processing Applications*. 2003.

43. R. E. Rosensweig, Basic Equations for Magnetic Fluids with Internal Rotations, in: S. Odenbach (Editor), *Ferrofluids:* Magnetically controllable fluids and their applications, Lecture Notes in Physics, Springer-Verlag, pp.61-84, 2002.

44. A. Tari, R. W. Chantrell, S. W. Charles and J. Popplewell, The Magnetic Properties and Stability of Ferrofluid Containing Fe_3O_4 particles, *Physica 97B* (1979) 57-64.1978

45. Ainhoa Urtizberea, Eva Natividad, Ana Arizaga, Miguel Castro, and Arturo Mediano, Specific Absorption Rates and Magnetic Properties of Ferrofluids with Interaction Effects at Low Concentrations. *J. Phys. Chem. C* 2010, *114,* 4916–4922.2010
46. Weber S, Dudzinski DT, Gu L, Mielke N, Casas F, Noecker AM, Saeed D, Ootaki Y, Fukamachi K, Smith WA, Duncan BW, The PediPump: a versatile, implantable pediatric ventricular assist device-update III. *ASAIO Journal*. 53(6):730-3, 2007 Nov-Dec.
47. Westerhof N, Elzinga G, Sipkema P, An artificial arterial system for pumping hearts. *Journal of Applied Physiology*. 31(5):776-81, 1971
48. Duncan, B.W., Dudzinski, D.T., Gu, L., Mielke, N., Noecker, A.M., Kopcak, M.W., Fukamachi, K., Cingoz, F., Ootaki, Y., and Smith, W.A. 2006. The PediPump: development status of a new pediatric ventricular assist device: update II. *ASAIO Journal* 52:581-587.
49. Harlow, James H. *Electric Power Transformer Engineering*. Boca Raton, FL: CRC, 2007
50. http://www.mathworks.com/products/simpower/, Matlab-Simulink, Mathworks, Natick, Massachusetts
51. Ogata, Katsuhiko. *Modern Control Engineering*. Upper Saddle River, NJ: Prentice Hall, 2002.